


Numerical investigation of electrostatic force density in ionic crystals such as NaCl

Vadim A. Markel ^{*}*Department of Radiology, University of Pennsylvania, Philadelphia, 19104 Pennsylvania, USA*

(Received 20 December 2022; revised 20 February 2023; accepted 22 March 2023; published 31 March 2023)

We investigate the density of electrostatic force in a continuous medium modeled as an ionic crystal similar to that of NaCl. The theoretical model is three-dimensional and consists of a lattice of ions of alternating signs. The ions can interact with each other and the externally applied electric field and pressure via elastic springs, which model short-range chemical bonds, and long-range Coulomb interactions. The condition of equilibrium can be solved numerically to yield the basic physical parameters of the structure including Young's modulus, the dielectric permittivity, and the electrically induced strain. We then compare these results to the theoretical predictions obtained according to various formulas for the electrostatic force density that can be found in the literature. It is shown that Helmholtz force density predicts the numerically computed strain almost perfectly while other expressions result in large errors. The numerical simulations are limited to statics.

DOI: [10.1103/PhysRevB.107.104307](https://doi.org/10.1103/PhysRevB.107.104307)

I. INTRODUCTION

Although the form of electromagnetic force density in continuous media is an old topic, it still continues to attract significant attention [1]. Many relevant works consider the general case of time-dependent fields in media with non-trivial electric and magnetic properties, but assume the objects to be absolutely rigid (except when interpreting experimental deflection of a flexible cantilever in terms of the applied force) [2–4]. In this case, only the total force acting on a material body is important. In a recent paper [5], we argued that the two main competing expressions for the force density (the standard Lorentz and the Einstein-Laub force densities [6]) are consistent with all conservation laws including conservation of energy, momentum, and linear motion of the center of energy of the system “object + field.” Therefore theoretical arguments cannot be used to determine which expression for the force density is correct. One of the formulations does result in a geometrical shift of the rigid object upon transmission of a transient pulse (the Balazs thought experiment), but this shift is compensated by the energy transferred from the field to the object. From the experimental point of view, it is doubtful that the geometrical shift mentioned above can be observed since the measurements are likely to be sensitive to the overall center of energy and, in addition, the geometrical shift in question is extremely small.

However, if we abandon the assumption of absolute rigidity, different theories for the force density would predict different elastic deformations, which can be verified in realistic experiments. To see the effect, it is sufficient to consider the simplest case of a non-magnetic dielectric in a static electric field. Things are somewhat complicated though because there are more than just two competing expressions for the force density that are applicable to this case. The two main com-

peting theories mentioned above (Lorentz and Einstein-Laub) result in the force densities denoted by $\mathbf{f}_d(\mathbf{r})$ and $\mathbf{f}_b(\mathbf{r})$ below. These densities integrate to the same total force under very general conditions, but predict different elastic deformations (as shown below, incorrectly). In addition, there are two more commonly encountered definitions of the force density, denoted below by $\mathbf{f}_c(\mathbf{r})$ and $\mathbf{f}_d(\mathbf{r})$, which predict the same total force as the former two under the assumptions of linearity and stationarity, but not more generally. On top of that, there also exists the electrostriction force $\mathbf{f}_{\text{elstr}}(\mathbf{r})$, which integrates to zero over the entire body and for this reason is often excluded from consideration (i.e., see Ref. [4]). Since $\mathbf{f}_{\text{elstr}}(\mathbf{r})$ always generates zero total force, it must be added to one of the above force densities. The special combination $\mathbf{f}_H(\mathbf{r}) = \mathbf{f}_c(\mathbf{r}) + \mathbf{f}_{\text{elstr}}(\mathbf{r})$ is known as the Helmholtz force density; the corresponding expression was derived for compressible fluids as early as in 1881 [7].

Given the uncertainty associated with the above choices, it is desirable to verify the predictions of various expressions for the force density not only experimentally but theoretically. An important step in this direction was made by Barnett and Loudon [8]. Reference [8] considers the force of attraction between a point charge and a dielectric half-space. However, as all tests that are based on the total force or torque, the test of Ref. [8] did not discriminate conclusively between the different expressions. It appears to be impossible to decide theoretically which of the competing force densities is correct while staying entirely within the framework of macroscopic electrodynamics. A more detailed microscopic model of the medium is needed.

In this paper, we construct and investigate numerically such a model. Briefly, the model consists of an ionic lattice similar to that of NaCl in which the ions are connected by short-range elastic forces that model the chemical bonds and can interact via the Coulomb interaction with each other and an externally applied field. External pressure can also be included into consideration. The model is purely classical but accounts

*vmarkel@upenn.edu

self-consistently for stability of matter, electric polarization and electro-mechanical phenomena such as electrostriction (since the considered structure has a center of symmetry, there is no piezoelectric effect; the latter can be introduced into the model by modifying the crystal geometry). Numerical simulations demonstrate conclusively that the only expression that predicts the elastic deformations correctly is the Helmholtz force density.

It should be noted that constructing a solvable classical model for a crystal is not a trivial task. In crystallography, atom layers or atom chains are often considered independently. For example, consideration of atom layers as homogeneously charged infinitely thin planes is the basis of the classical Tasker condition of stability [9] telling which kinds of crystal surfaces are stable. Some theories also consider independent or quasi-independent chains of ions [10]. In the model of this paper, it is essential that ions are treated as discrete and that all interactions including the lateral bonds are taken into account. Therefore although we also consider equivalent chains of ions, all ions are coupled by various forces and all relevant interactions are taken into account in three dimensions.

The paper is organized as follows. In Sec. II, we review the competing expressions for the force density and establish mathematical relations between these expressions. In particular, it is shown that, in statics, all these expressions predict the same total force but different elastic deformations. In Sec. III, we describe a thought experiment in which a material slab is placed in a constant electric field and summarize the predictions for the electrically induced surface pressure that follow from the various force densities. In Sec. IV, we describe the microscopic model of an ionic crystal that is used to test the theoretical predictions. In Sec. V, we give a detailed mathematical description of all forces that are included in the model. Section VI describes the numerical algorithms that are used to find the equilibrium positions of the ions at given values of externally applied electric field and pressure. Section VII presents the results of numerical simulations of the basic physical properties of the model structure, which include the lattice unit, Young's modulus, the dielectric permittivity, and the electrostrictive coefficient. Sec. VIII presents the central result of this paper. Here we compare the numerically computed strain induced by an external electric field to various theoretical predictions and show that the Helmholtz force density provides the best (and very accurate) fit. Finally, Sec. IX contains a brief discussion. Appendix contains expressions that generalize Helmholtz force density beyond the assumptions adopted in this paper. Reference [11] contains a computational package, scripts and instructions, which can be used to regenerate all data used in the plots below and to rebuild graphics, as well as to run similar custom simulations.

Gaussian system of units is used throughout the paper. However, figures display only dimensionless quantities and therefore are not affected by this choice.

II. COMPETING EXPRESSIONS

We consider a solid, elastically deformable, finite dielectric body embedded in vacuum. The dielectric can be polarized by an externally applied electric field. The two most frequently

encountered expressions for the force density acting in such objects are

$$\mathbf{f}_a(\mathbf{r}) = -(\nabla \cdot \mathbf{P}(\mathbf{r})) \mathbf{E}(\mathbf{r}), \quad (1a)$$

$$\mathbf{f}_b(\mathbf{r}) = (\mathbf{P}(\mathbf{r}) \cdot \nabla) \mathbf{E}(\mathbf{r}), \quad (1b)$$

where $\mathbf{P}(\mathbf{r})$ is the vector of electric polarization and $\mathbf{E}(\mathbf{r})$ is the electric field. Since we consider in this paper static fields, time dependence is omitted in the notations. We emphasize that $\mathbf{E}(\mathbf{r})$ in (1) is the total electric field rather than its external (applied) component. The distinction is important. Indeed, the *total* force acting on a finite body can be computed as the force exerted by the applied field on the induced charges whereas the internal forces cancel out by Newton's third law. However, if we are interested in the *density* of force, it is not correct to disregard internal interactions. Consequently, the total electric field must be used in (1).

As was noted by Barnett and Loudon [8], the expression (1a) is based on "treating the medium as formed from individual charges" while the second expression (which can be viewed as more conventional since it appears in many textbooks) is based on "treating the medium as being formed from individual dipoles". Indeed, $-\nabla \cdot \mathbf{P}(\mathbf{r})$ is the conventional expression for the induced electric charge density. Therefore (1a) is a continuous version of Coulomb's law. The expression (1b) is derived differently. Here one assumes that a volume element δV drawn around the point \mathbf{r} has the dipole moment $\delta \mathbf{d}(\mathbf{r}) = \mathbf{P}(\mathbf{r})\delta V$. Then the element of force acting on δV is computed as $\delta \mathbf{F}(\mathbf{r}) = (\delta \mathbf{d}(\mathbf{r}) \cdot \nabla) \mathbf{E}(\mathbf{r})$, and the differential density of force as $\mathbf{f}(\mathbf{r}) = \delta \mathbf{F}(\mathbf{r})/\delta V$, which leads to (1b).

However, the physical reasoning behind the expressions in (1) is flawed. Consider first (1a). The direct application of Coulomb's law to the induced charge density, on which this formula is based, ignores the fact that, classically (that is, without quantum mechanics), a system of charged particles cannot hold itself together in a stable equilibrium. We must therefore introduce, in addition to $\mathbf{f}_a(\mathbf{r})$, some phenomenological force density to account for stability of matter. This force density will integrate to zero over the whole dielectric, but it cannot be disregarded locally, and must therefore be included in the definition of $\mathbf{f}(\mathbf{r})$. Consequently, (1a) is not the complete expression. The formula (1b) can also be challenged. First, the physical picture of a continuous medium consisting of rigid dipoles is simplistic and in some cases plainly incorrect. Second, there is no reason to treat the bonds that hold charges in a dipole together as absolutely rigid. Finally, there still remains the question of what force holds the dipoles together. Thus, in both cases, some additional forces must be introduced, and which part of these forces is purely elastic (i.e., can be related directly to the elastic strain for zero applied field) and which is induced by the applied electric field is not possible to tell without introducing a more detailed microscopic model of the medium.

Before proceeding, it is instructive to consider the total force acting on the dielectric body, which is defined by the spatial integral

$$\mathbf{F}_{\text{tot}} = \int \mathbf{f}(\mathbf{r}) d^3 r. \quad (2)$$

A necessary condition for any expression for the force density to be correct is that it predict the total force correctly. Both expressions in (1) satisfy this condition for static or slowly varying fields [12]. This can be seen most easily from (1a), since any force density that can be added to it is necessarily internal and, therefore, would cancel out by Newton's third law when integrated according to (2). We can make an even stronger statement: $\mathbf{f}_a(\mathbf{r})$ and $\mathbf{f}_b(\mathbf{r})$ integrate to the same instantaneous value (now, not necessarily the total force acting on the body) for arbitrary time-dependent fields, arbitrary nonlinear relation between $\mathbf{P}(\mathbf{r})$ and $\mathbf{E}(\mathbf{r})$, or even in the hypothetical case when there is no such deterministic relation. All that is required is that $\mathbf{P}(\mathbf{r})$ vanish in vacuum. Indeed, $\mathbf{f}_a(\mathbf{r})$ and $\mathbf{f}_b(\mathbf{r})$ differ by divergence of a tensor:

$$\mathbf{f}_b(\mathbf{r}) = \mathbf{f}_a(\mathbf{r}) + \nabla \cdot \hat{T}_1(\mathbf{r}), \quad (3)$$

where

$$\hat{T}_1(\mathbf{r}) = \mathbf{P}(\mathbf{r}) \otimes \mathbf{E}(\mathbf{r}). \quad (4)$$

Here the symbol \otimes denotes tensor product and we have adopted the convention according to which

$$(\nabla \cdot \hat{T}(\mathbf{r}))_i = \sum_j \frac{\partial T_{ji}(\mathbf{r})}{\partial r_j}. \quad (5)$$

The divergence term in (3) integrates to zero over any finite body as long as $\mathbf{P}(\mathbf{r})$ vanishes in vacuum. Consequently, spatial integrals of $\mathbf{f}_a(\mathbf{r})$ and $\mathbf{f}_b(\mathbf{r})$ are the same.

The above example suggests that we can generate additional expressions for $\mathbf{f}(\mathbf{r})$ that predict the same \mathbf{F}_{tot} by exploring the transformation $\mathbf{f}(\mathbf{r}) \rightarrow \mathbf{f}(\mathbf{r}) + \nabla \cdot \hat{T}(\mathbf{r})$. In (3), we have taken $\hat{T}(\mathbf{r}) = \hat{T}_1(\mathbf{r})$ where $\hat{T}_1(\mathbf{r})$ is defined in (4). Assuming that $\hat{T}(\mathbf{r})$ is quadratic in the fields $\mathbf{E}(\mathbf{r})$, $\mathbf{P}(\mathbf{r})$, and contains no additional parameters related to properties of the medium, the only other choice (up to a numerical factor) is

$$\hat{T}_2(\mathbf{r}) = -\frac{1}{2}(\mathbf{P}(\mathbf{r}) \cdot \mathbf{E}(\mathbf{r}))\hat{I}, \quad (6)$$

where \hat{I} is the unit tensor and the minus sign has been introduced for convenience. Although the expression (6) is simple, it cannot be developed into anything looking familiar in general. However, we can obtain simplifications by utilizing the assumptions of linearity and stationarity [13]. According to the first assumption, $\mathbf{P}(\mathbf{r}) = \chi(\mathbf{r})\mathbf{E}(\mathbf{r})$, where $\chi(\mathbf{r}) = [\epsilon(\mathbf{r}) - 1]/4\pi$ and $\epsilon(\mathbf{r})$ is the dielectric permittivity of the medium. The condition of stationarity can be written as $\nabla \times \mathbf{E}(\mathbf{r}) = 0$. Under these assumptions, we have

$$\nabla \cdot \hat{T}_2(\mathbf{r}) = -\frac{E^2(\mathbf{r})}{8\pi}\nabla\epsilon(\mathbf{r}) - \chi(\mathbf{r})(\mathbf{E}(\mathbf{r}) \cdot \nabla)\mathbf{E}(\mathbf{r}). \quad (7)$$

To see that (7) is correct, consider the following chain of equalities:

$$\nabla \cdot \hat{T}_2(\mathbf{r}) = -\frac{1}{2}\nabla(\mathbf{P}(\mathbf{r}) \cdot \mathbf{E}(\mathbf{r})) \quad (8a)$$

$$= -\frac{1}{2}\nabla(\chi(\mathbf{r})E^2(\mathbf{r})) \quad (8b)$$

$$= -\frac{E^2(\mathbf{r})}{2}\nabla\chi(\mathbf{r}) - \frac{1}{2}\chi(\mathbf{r})\nabla E^2(\mathbf{r}) \quad (8c)$$

$$= -\frac{E^2(\mathbf{r})}{8\pi}\nabla\epsilon(\mathbf{r}) - \chi(\mathbf{r})(\mathbf{E}(\mathbf{r}) \cdot \nabla)\mathbf{E}(\mathbf{r}). \quad (8d)$$

In transitioning from (8a) to (8b), we have used the assumption of linearity and in transitioning from (8c) to (8d), we have used the vector identity $\nabla E^2(\mathbf{r}) = 2(\mathbf{E}(\mathbf{r}) \cdot \nabla)\mathbf{E}(\mathbf{r})$, which holds for irrotational fields. Evaluating $\mathbf{f}_b(\mathbf{r})$ to the same level of approximation (in this case, using only linearity), we find that

$$\mathbf{f}_c(\mathbf{r}) \stackrel{\text{def}}{=} \mathbf{f}_b(\mathbf{r}) + \nabla \cdot \hat{T}_2(\mathbf{r}) = -\frac{E^2(\mathbf{r})}{8\pi}\nabla\epsilon(\mathbf{r}). \quad (9)$$

This is another frequently encountered expression for the density of force.

We will refer below to $\mathbf{f}_a(\mathbf{r})$, $\mathbf{f}_b(\mathbf{r})$, and $\mathbf{f}_c(\mathbf{r})$ as to expansion forces as they, generally, try to increase the volume of a dielectric. There exists another kind of force density, known as electrostriction, which does the opposite. However, to define this force, we must introduce an additional medium parameter $\alpha(\mathbf{r})$, which does not appear directly in Maxwell's equations or in the electromagnetic constitutive relations. Namely, let

$$\hat{T}_{\text{elstr}}(\mathbf{r}) = \frac{1}{8\pi}\alpha(\mathbf{r})E^2(\mathbf{r})\hat{I}. \quad (10)$$

The force density associated with $\hat{T}_{\text{elstr}}(\mathbf{r})$,

$$\mathbf{f}_{\text{elstr}}(\mathbf{r}) = \nabla \cdot \hat{T}_{\text{elstr}}(\mathbf{r}) = \frac{1}{8\pi}\nabla[\alpha(\mathbf{r})E^2(\mathbf{r})], \quad (11)$$

is known as the electrostriction force. The coefficient $\alpha(\mathbf{r})$, which gives induced *stress* in terms of the electric field, can be referred to as the electrostrictive coefficient. However, it is more conventional to reserve this term for the coefficient $\mu(\mathbf{r})$, which gives the induced *strain* [14]. In the case of uniaxial or uniform compression or dilation, the two coefficients are related quite simply as $\alpha = \mu\eta$, where η is Young's modulus. A more general relation applicable to solids is given in Appendix. We will use the term "electrostriction coefficient" for both α and μ in this paper.

While the electrostriction coefficient is an independent property of the medium, it can be shown that $\alpha(\mathbf{r})$ and $\epsilon(\mathbf{r})$ are related as

$$\alpha(\mathbf{r}) = \rho(\mathbf{r})\frac{\partial\epsilon(\mathbf{r})}{\partial\rho(\mathbf{r})}, \quad (12)$$

where $\rho(\mathbf{r})$ is the mass density, the derivative must be computed at a fixed temperature, and the density is assumed to change as a result of uniform or uniaxial compression or dilation. Equation (12) can be viewed as the operational definition of $\alpha(\mathbf{r})$. That is, if $\epsilon(\mathbf{r})$ can be measured or simulated at different levels of strain, we can use (12) to determine $\alpha(\mathbf{r})$. This approach is adopted in the simulations below. Note that $\alpha(\mathbf{r})$ is not well defined by (12) if $\rho(\mathbf{r}) = 0$. We should, however, require on physical grounds that $\alpha(\mathbf{r})$ vanish in vacuum. Then $\mathbf{f}_{\text{elstr}}(\mathbf{r})$ integrates to zero over the entire body. It follows that $\mathbf{f}_{\text{elstr}}(\mathbf{r})$ cannot be the complete expression for the electrically induced force density; rather, it must be added to one of the expansion forces $\mathbf{f}_a(\mathbf{r})$, $\mathbf{f}_b(\mathbf{r})$, or $\mathbf{f}_c(\mathbf{r})$.

One such combination is of particular significance. Adding together $\mathbf{f}_c(\mathbf{r})$ and $\mathbf{f}_{\text{elstr}}(\mathbf{r})$ with $\alpha(\mathbf{r})$ defined in (12), we obtain

what is known as the Helmholtz force density.

$$\begin{aligned} \mathbf{f}_H(\mathbf{r}) &\stackrel{\text{def}}{=} \mathbf{f}_c(\mathbf{r}) + \mathbf{f}_{\text{elstr}}(\mathbf{r}) \\ &= \frac{1}{8\pi} \left\{ \nabla \left[\rho(\mathbf{r}) \frac{\partial \epsilon(\mathbf{r})}{\partial \rho(\mathbf{r})} E^2(\mathbf{r}) \right] - E^2(\mathbf{r}) \nabla \epsilon(\mathbf{r}) \right\}. \end{aligned} \quad (13)$$

Expression (13) was derived by Helmholtz in 1881 [7] for the case compressible fluids from a combination of thermodynamic and virtual work principles. Many contemporary textbooks expound this derivation, see Refs. [[15], §6.6], [[16], §2.13], and [[17], §15]. The key idea here is that the change of internal energy of a dielectric due to the dependence of its permittivity on the strain is not negligible in comparison to other similar terms. Correspondingly, the electrostriction force is not negligible in comparison to other commonly considered forces. Note that (13) relies on the assumptions of linear local relation between $\mathbf{P}(\mathbf{r})$ and $\mathbf{E}(\mathbf{r})$ [as it contains $\epsilon(\mathbf{r})$ explicitly] and uniform or uniaxial strain. The model considered below satisfies these conditions. More general relations for the electrostriction and Helmholtz forces are adduced in Appendix.

As noted above, the electrostrictive coefficient $\alpha(\mathbf{r})$ does not appear in Maxwell's equations or in constitutive relations and cannot be, in general, expressed in terms of $\epsilon(\mathbf{r})$ itself (rather than in terms of its derivatives). However, in the special case of a simple relation between $\epsilon(\mathbf{r})$ and $\rho(\mathbf{r})$ of the form

$$\epsilon(\mathbf{r}) = 1 + \beta \rho(\mathbf{r}), \quad (14a)$$

where β is some constant, we have

$$\alpha(\mathbf{r}) = \epsilon(\mathbf{r}) - 1. \quad (14b)$$

The dependence (14a) is characteristic of gases rather than solids [and thus assumes that $\epsilon(\mathbf{r}) - 1$ is small], but we can use the result (14b) formally in (12) to obtain the following approximate expression for the electrostriction force:

$$\mathbf{f}_{\text{elstr}}^{(\text{appr})}(\mathbf{r}) = \nabla \left[\frac{\epsilon(\mathbf{r}) - 1}{8\pi} E^2(\mathbf{r}) \right]. \quad (15)$$

We can further use (15) to generate yet another familiar-looking expression for the force density by writing

$$\begin{aligned} \mathbf{f}_d(\mathbf{r}) &\stackrel{\text{def}}{=} \mathbf{f}_H^{(\text{appr})}(\mathbf{r}) \\ &= \mathbf{f}_c(\mathbf{r}) + \mathbf{f}_{\text{elstr}}^{(\text{appr})}(\mathbf{r}) = \frac{\epsilon(\mathbf{r}) - 1}{8\pi} \nabla E^2(\mathbf{r}). \end{aligned} \quad (16)$$

In writing (16), we have already adopted the linear approximation (or else $\epsilon(\mathbf{r})$ would not be a good characteristic of the medium). If we, in addition, assume stationarity so that the electric field is irrotational, then it is easy to show that $\mathbf{f}_d(\mathbf{r}) = \mathbf{f}_b(\mathbf{r})$. Thus $\mathbf{f}_b(\mathbf{r})$ and $\mathbf{f}_d(\mathbf{r})$ can be viewed as low-density approximation of the Helmholtz force, $\mathbf{f}_H^{(\text{appr})}(\mathbf{r})$.

We can also use in (12) a slightly more complicated relation between $\epsilon(\mathbf{r})$ and $\rho(\mathbf{r})$ of the form

$$\epsilon(\mathbf{r}) = \frac{1 + 2\beta\rho(\mathbf{r})}{1 - \beta\rho(\mathbf{r})}, \quad (17a)$$

which is known as the Clausius-Mossotti approximation. This yields

$$\alpha(\mathbf{r}) = (\epsilon(\mathbf{r}) - 1) \frac{\epsilon(\mathbf{r}) + 2}{3}. \quad (17b)$$

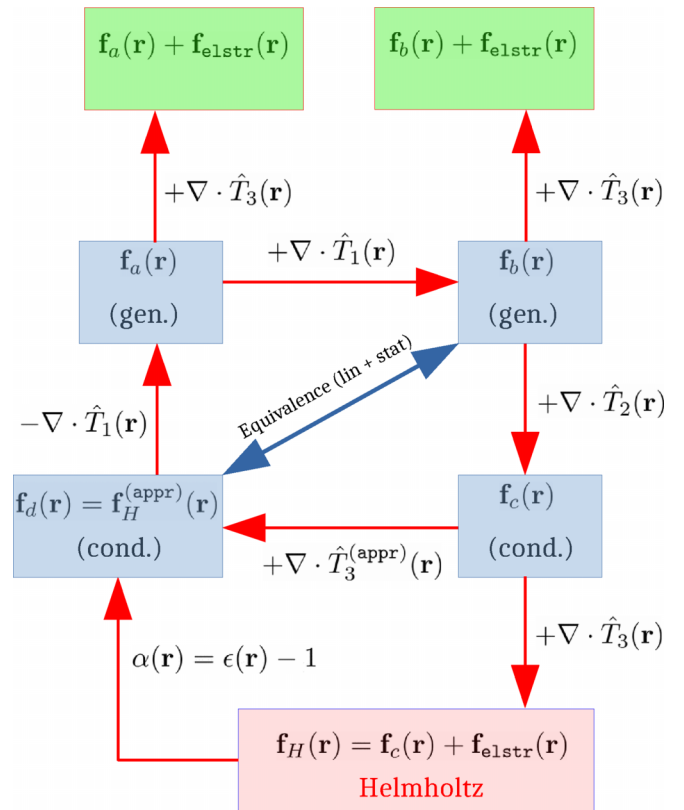


FIG. 1. Schematic relationship between various force densities discussed in Sec. II. The expansion forces $\mathbf{f}_a(\mathbf{r})$, $\mathbf{f}_b(\mathbf{r})$, $\mathbf{f}_c(\mathbf{r})$, and $\mathbf{f}_d(\mathbf{r})$ can be obtained from each other by adding divergences of tensors as indicated by the arrows and the accompanying labels. The densities labeled as “(gen.)” yield the same total force for general fields; those labeled “(cond.)” require linearity and stationarity in order to predict the same total force as $\mathbf{f}_a(\mathbf{r})$ and $\mathbf{f}_b(\mathbf{r})$. Equivalence between $\mathbf{f}_d(\mathbf{r})$ and $\mathbf{f}_b(\mathbf{r})$ holds only under the assumptions of linearity and stationarity.

However, adding (17b) to any of the expansion force densities $\mathbf{f}_a(\mathbf{r})$, $\mathbf{f}_b(\mathbf{r})$ or $\mathbf{f}_c(\mathbf{r})$ does not result in a familiar or commonly used formula.

It is useful to keep in mind that, unlike the piezoelectric effect, electrostriction is not reciprocal. In other words, applied electric field can cause strain but applying external pressure does not induce electric field or polarization of the dielectric. This is evident already from the quadratic dependence of the electrostriction force density on the electric field. Also, if the dielectric is internally homogeneous, the force densities $\mathbf{f}_a(\mathbf{r})$ and $\mathbf{f}_c(\mathbf{r})$ are applied only at the surface. However, the forces $\mathbf{f}_b(\mathbf{r})$, $\mathbf{f}_d(\mathbf{r})$, $\mathbf{f}_{\text{elstr}}(\mathbf{r})$, and $\mathbf{f}_H(\mathbf{r})$ do not generally vanish in the bulk of a homogeneous medium.

The schematic relation between all expressions for the force density that were introduced above is illustrated in Fig. 1. There are four expansion force densities, $\mathbf{f}_a(\mathbf{r})$, $\mathbf{f}_b(\mathbf{r})$, $\mathbf{f}_c(\mathbf{r})$, and $\mathbf{f}_d(\mathbf{r})$. Under the assumptions of linearity and stationarity, $\mathbf{f}_d(\mathbf{r})$ is equivalent to $\mathbf{f}_b(\mathbf{r})$. Under the same conditions, the expansion force densities predict the same total force \mathbf{F}_{tot} . One can add to any of the expansion forces the electrostriction force density $\mathbf{f}_{\text{elstr}}(\mathbf{r})$ without affecting \mathbf{F}_{tot} . Accounting for the equivalence of $\mathbf{f}_d(\mathbf{r})$ and $\mathbf{f}_b(\mathbf{r})$, which we assume, this creates six distinct possibilities for the force

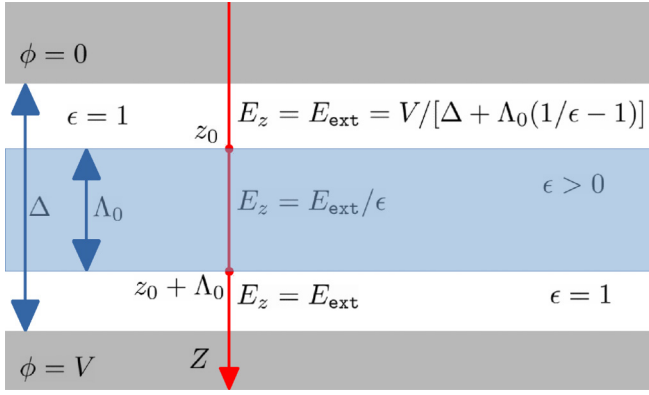


FIG. 2. Schematic illustration of the proposed setup. A dielectric slab of width Λ_0 is placed in a uniform, normally directed electric field \mathbf{E}_{ext} .

density. One of these possibilities, obtained by adding $\mathbf{f}_c(\mathbf{r})$ and $\mathbf{f}_{\text{elstr}}(\mathbf{r})$, is special and known as the Helmholtz force density $\mathbf{f}_H(\mathbf{r})$. If we make the approximation $\alpha(\mathbf{r}) = \epsilon(\mathbf{r}) - 1$ in the expression (13) for $\mathbf{f}_H(\mathbf{r})$, the force density $\mathbf{f}_d(\mathbf{r})$ is obtained. We emphasize that shown in Fig. 1 are not *all* possible forms of the force density that are consistent with the total force \mathbf{F}_{tot} as predicted by $\mathbf{f}_d(\mathbf{r})$ or $\mathbf{f}_b(\mathbf{r})$, which we assume to be generally correct. Rather, Fig. 1 summarizes various competing expressions that appear in the literature.

In what follows, we assume that, in the absence of external pressure or electric field, the dielectric is homogeneous and characterized by some constant values ρ , ϵ , and α , so that we can write

$$\alpha(\mathbf{r}) = \alpha\theta(\mathbf{r}), \quad \epsilon(\mathbf{r}) = 1 + (\epsilon - 1)\theta(\mathbf{r}), \quad (18)$$

etc., where $\theta(\mathbf{r})$ is the shape function: it is 1 inside the dielectric and 0 in vacuum. In general, when write $\epsilon(\mathbf{r})$ or $\epsilon(z)$, etc., we imply a spatially varying quantity whereas when the argument is omitted, as in ϵ , it is the constant value inside the material.

III. ELECTRICALLY INDUCED PRESSURE ON A DIELECTRIC SLAB

In Ref. [8], Barnett and Loudon considered the static force of attraction between a point charge and a dielectric half-space. The force densities $\mathbf{f}_a(\mathbf{r})$ and $\mathbf{f}_b(\mathbf{r})$ predicted the same total force. The force density $\mathbf{f}_c(\mathbf{r})$ was not considered, but it would have predicted the same result, and we know that $\mathbf{f}_d(\mathbf{r})$ is equivalent to $\mathbf{f}_b(\mathbf{r})$ under the assumptions of Ref. [8]. As electrostriction does not generate a total force, its inclusion would not have influenced the results. More recently, Park *et al.* showed that the lateral pulling force on a dielectric slab partially inserted in a flat capacitor is the same for different expressions for the force density [18]. These results are consistent with the derivations of Sec. II where we have shown that all competing expressions for the force density differ by divergence of a tensor and therefore predict the same total force. However, different force densities predict different elastic deformations, and this effect will be explored below.

Consider the simple setup illustrated in Fig. 2. Here a flat capacitor of width Δ is charged to a potential difference V . A dielectric slab of the width $\Lambda_0 < \Delta$ and dielectric

TABLE I. Three-dimensional form, projection onto the Z axis in the setup of Fig. 2, and the electrically induced surface pressure Π_{ind} [see Eq. (19) and Fig. 2] for various force densities introduced in Sec. II. Positive pressure implies compression and negative pressure implies extension of the slab. Linearity and stationarity are assumed. Line H corresponds to the Helmholtz force density (13). One-dimensional projections of the force density have been written accounting for the condition $d[\epsilon(z)E_z(z)]/dz = 0$.

Force	3D, $\mathbf{f}(\mathbf{r})$	1D, $f_z(z)$	Π_{ind}
(a)	$-(\nabla \cdot \mathbf{P})\mathbf{E}$	$\frac{1}{8\pi} \frac{d}{dz} E_z^2(z)$	$-\frac{E_{\text{ext}}^2}{8\pi} \frac{\epsilon^2 - 1}{\epsilon^2}$
(b) and (d)	$(\mathbf{P} \cdot \nabla)\mathbf{E}$	$\frac{\epsilon(z) - 1}{8\pi} \frac{d}{dz} E_z^2(z)$	$-\frac{E_{\text{ext}}^2}{8\pi} \frac{(\epsilon - 1)^2}{\epsilon^2}$
(c)	$-\frac{E^2}{8\pi} \nabla \epsilon$	$-\frac{1}{8\pi} E_z^2(z) \frac{d}{dz} \epsilon(z)$	$-\frac{E_{\text{ext}}^2}{8\pi} \frac{\epsilon - 1}{\epsilon}$
elstr	$\frac{1}{8\pi} \nabla(\alpha E^2)$	$\frac{1}{8\pi} \frac{d}{dz} \alpha(z) E_z^2(z)$	$\frac{E_{\text{ext}}^2}{8\pi} \frac{\alpha}{\epsilon^2}$
H	(c) + (elstr)	(c) + (elstr)	$\frac{E_{\text{ext}}^2}{8\pi} \frac{\alpha - (\epsilon - 1)\epsilon}{\epsilon^2}$

constant ϵ is inserted in the capacitor. Here Λ_0 is the slab width in the absence of external electric field and pressure; a more general notation that accounts for possible elastic deformations will be introduced below. The electric field is perpendicular to the slab. In the vacuum gaps, the field is $E_z = E_{\text{ext}} = V/[\Delta + \Lambda_0(1/\epsilon - 1)]$ and inside the dielectric it is $E_z = E_{\text{ext}}/\epsilon$. Without loss of generality, we can assume that the applied field E_{ext} is the mathematically independent variable that can be controlled in an experiment. In this setup, the total force acting on the slab is zero. However, different expressions for the force density predict different values of the electrically induced pressure on the surfaces of the slab as is summarized in Table I. Note that, in the geometry of Fig. 2, all force densities have nonzero contributions only on the slab surfaces and vanish in the bulk. The electrically induced pressure on the slab at the surface $z = z_0$ is defined as

$$\Pi_{\text{ind}} = \int_{z_0 - \delta}^{z_0 + \delta} f_z(z) dz, \quad (19)$$

where $f_z(z)$ is listed in the third column of Table I and δ is an infinitesimally small constant. Here we have used the Greek letter Π to distinguish pressure from the electric polarization of the medium. The small constant δ has been introduced to account for the fact that the function $f_z(z)$ has a singularity exactly at $z = z_0$ and is zero elsewhere. Since this singularity can be always represented as derivative of a discontinuous function, integration by parts can be used to evaluate (19). This approach is consistent with other methods such as defining the singular contributions directly and then working with generalized functions according to usual rules or introducing a smooth transition layer and thus avoiding singularities altogether. The pressure on the opposite face of the slab exactly counteracts Π_{ind} so that the total force on the slab is zero. Note that, assuming that $\epsilon > 1$ and $\alpha > 0$, the electrostriction force predicts a positive pressure (leading to a contraction of

the slab) while all expansion forces predict negative pressures (leading to an expansion).

In what follows, we will devise a microscopic model of the medium in which the Young modulus, the dielectric constant, the electrostrictive coefficient and the relative extension or contraction of the slab under an applied electric field can be directly computed. Comparing the latter result to the theoretical predictions obtained from the induced surface pressures summarized in Table I and the computed Young's modulus, we will be able to tell which expression for the force density is more consistent with the simulations.

IV. MICROSCOPIC MODEL

We now describe a microscopic model, which will be used to test the theoretical predictions summarized in Table I. We consider an ionic crystal similar to that of NaCl and consisting of N atom layers as shown in Fig. 3. The ions are pointlike and have the electric charges $\pm q$ where $q > 0$ for definitiveness. The structure is infinite in the X and Y directions but finite in Z . In principle, the number of layers N can be even or odd. Asymmetric termination (with an odd N) does not contradict the classical stability requirement of Tasker [9]. However, since physical properties of the crystal are not expected to depend on the termination, we consider below only even N . In Fig. 3, a symmetric termination with an even N is shown.

The following forces are included in the model. First, the neighboring ions are connected by harmonic springs, which model chemical bonds. The equilibrium length of each spring is h and the spring constant is k . Thus each ion, except for those in the surface layers $n = 1$ and $n = N$, is connected by springs to six other ions. Those on the surface have only five such connections. In addition, the ions can interact electrostatically with each other and with the external electric field \mathbf{E}_{ext} , which we assume to be constant and directed along Z . Finally, we can apply some phenomenological non-electromagnetic forces to the surface layer ions in order to model external pressure Π_{ext} .

Given the interactions described above, the model is completely characterized by the single scalar parameter

$$\kappa = q^2/kh^3. \quad (20)$$

The parameter κ quantifies the strength of electrostatic interaction of the ions relative to the stiffness of the lattice. In the limit $\kappa \rightarrow 0$, the crystal is not polarizable and has the dielectric constant $\epsilon = 1$. Note that we could simplify the model by considering a finite charge q (so that there is still interaction with the applied field) but disregarding electrostatic interactions of the ions. The crystal in this simplified model can be deformed by the applied field but is not polarizable, so that its $\epsilon = 1$ regardless of κ . Therefore accounting for the electrostatic interactions is essential for the model to describe a polarizable dielectric.

As illustrated in Fig. 3(a), we assume that the ion positions make a perfect square lattice of unit step h in the XY plane regardless of the applied field. We will see below that, even in the absence of applied field, the equilibrium lattice step in the Z direction, denoted by u , is smaller than h due to electrostatic interactions of the layers. Consequently, the unit cell of the structure is not cubic. This is different from the real NaCl

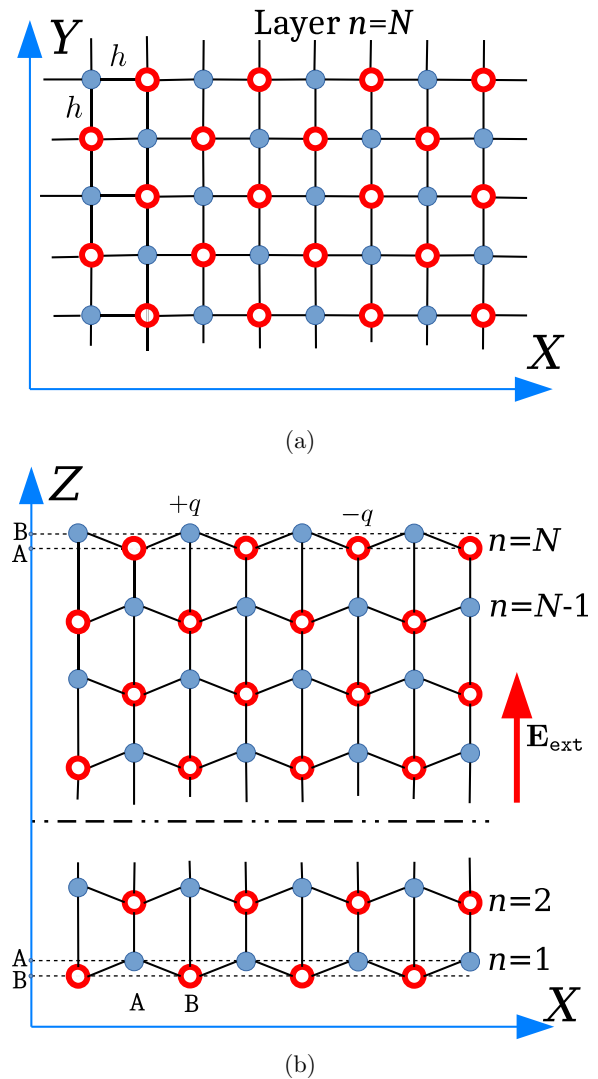


FIG. 3. Schematic illustration of the model. The structure consists of N infinite layers of ions stacked in the Z direction to form a slab. Positive ions of the charge $+q$ are shown by blue (filled) circles and negative ions of the charge $-q$ by red (open) circles. The X and Y coordinates of all ions lie on a square lattice of the step h while the Z coordinates can be displaced from the square lattice nodes by the external field \mathbf{E}_{ext} and electrostatic interactions. The letters A and B label sublattices and chains of ions (see text). (a) XY plane (layer $n = N$, top view) and (b) XZ plane.

crystals. The reason for this discrepancy is that we do not allow motion of the ions in the lateral directions as this would be too difficult to simulate. To justify the assumption, we can imagine that the edges of a large, square-shaped slab are glued rigidly to the planes $x = \pm R/2$, $y = \pm R/2$, where $R \gg \Lambda_0$, so that the lattice step in the XY plane is fixed to h . However, the ions far away from these fixation planes can move in the Z direction under the action of all forces mentioned above. Then the equilibrium Z coordinates of the ions are not required to be on a lattice. In particular, the unit cells that are close to the surfaces are different from those deep in the bulk. Similar dependence is known to exist in real crystals where the cells adjacent to the crystalline surfaces, edges and corners are

different from each other and from those in the bulk [19–21]. Still, in slabs with many atom layers, the equilibrium lattice unit u is well defined as is shown in Sec. VII A below.

Although we do not consider motion of the ions in the XY plane, the model is still three-dimensional as we account for the interactions of all pointlike ions. This is different from the, essentially, one-dimensional models in which a crystal is viewed as a stack of homogeneous planes [9] or an array noninteracting chains [10].

Each ion in the structure belongs to an atom layer n , to one of two sublattices of that layer, and also to a chain of ions, where chains are one-dimensional substructures parallel to the Z -axis. We will distinguish between two types of sublattices and two types of chains.

Consider first the sublattices. Each atom layer can be partitioned into two square sublattices of the step $\sqrt{2}h$, so that each sublattice contains ions of the same charge and all ions in a given sublattice have the same Z coordinate, even in the presence of an applied field. Assume for definiteness that the positive and negative ions of the layer $n = 1$ form the sublattices A and B, respectively. Then the odd-numbered layers have positive ions in sublattices A and negative ions in sublattices B. Conversely, even-numbered layers have negative ions in the sublattices A and positive ions in the sublattices B. Thus, assuming N is even, the negative ions shown in Fig. 3(a) by open red circles form the sublattice A while the positive ions (filled blue circles) form the sublattice B. The applied electric field can shift the sublattices of a given atom layer with respect to each other along the Z -axis as is shown in Fig. 3(b). However, two sublattices belonging to the same layer are connected by electrostatic attraction and lateral springs, which do not allow this displacement to become too large. Without any of these forces, the structure would be unstable.

Likewise, we can define chains of ions of the types A and B. An A-type chain has a positive ion in the atom layer $n = 1$ and a negative ion in the layer $n = N$. A B-type chain has a negative ion in the layer $n = 1$ and a positive ion in the layer $n = N$. All ions in an A-type chain belong to A-type sublattices, and all ions in A-type sublattices belong to A-type chains; a similar relation holds for the B-type sublattices and chains. This classification is illustrated in Fig. 3(b). All chains of the same type are equivalent, and we denote the Z coordinates of ions in the A-type and B-type chains by z_n^A and z_n^B , respectively. The same coordinates divided by h and thus dimensionless are denoted as $\xi_n^A = z_n^A/h$ and $\xi_n^B = z_n^B/h$.

Depending on polarity, an applied electric field will contract the chains of one type and expand the chains of the other type. In Fig. 3(b), the applied field contracts the A-type chains and extend the B-type chains. If we consider each chain in isolation for a large N and a nonzero applied field, the equilibrium lengths of the different-type chains can differ by more than h . This cannot happen in real crystals and is inconsistent with mechanical stability. However, the lateral bonds and the electrostatic interaction of sublattices counter-act the applied field and do not allow the length difference to become large. Therefore it is incorrect to consider the chains in isolation; rather, we must account for all the interactions that were introduced above self-consistently.

V. DEFINITION OF DIMENSIONLESS FORCES

In this section, we define all forces in units of the atomic force $F_{\text{at}} = kh$. Since we will be looking for the condition of equilibrium where the net force acting on each ion is zero, the units in which the forces are expressed are unimportant. It is however useful to keep in mind that the actual physical force is obtained by multiplying the expressions given below by F_{at} .

A. Internal electrostatic forces

Consider an arbitrary test ion located at the normalized depth $\xi = z/h$. The electrostatic force exerted by all other ions onto the test ion can be represented as a sum over all sublattices *except for the one to which the test ion belongs*. The force exerted on any ion by its own sublattice is obviously zero. Let there be a sublattice of an arbitrary type at the normalized depth $\xi' \neq \xi$. We denote the *absolute value* of the force exerted by this sublattice on the test ion by $\mathcal{F}_s(\xi, \xi')$ or $\mathcal{F}_d(\xi, \xi')$ where s and d stand for “same” and “different.” The subscript s indicates that the test ion at ξ is in a sublattice of the same type as the one at ξ' and d indicates that the two sublattices are of different types. We have by a direct calculation

$$\mathcal{F}_{s,d}(\xi, \xi') = \kappa \Sigma_{s,d}(|\xi - \xi'|), \quad (21a)$$

where the model parameter κ is defined in (20) and

$$\Sigma_s(\ell) = \sum_{m,n=-\infty}^{\infty} \frac{\ell}{[2(m^2 + n^2) + \ell^2]^{3/2}}, \quad (21b)$$

$$\Sigma_d(\ell) = \sum_{m,n=-\infty}^{\infty} \frac{\ell}{[2m(m-1) + 2n(n-1) + 1 + \ell^2]^{3/2}}. \quad (21c)$$

Here $\ell = |\xi - \xi'| = |z - z'|/h$.

A few comments are necessary at this point. First, $\mathcal{F}_{s,d}(\xi, \xi')$ and $\Sigma_{s,d}(\ell)$ are positive by definition. Projection of the force onto the Z axis can be positive or negative depending on ξ, ξ' and signs of the charges involved. This will be accounted for below. Second, as mentioned above, own sublattice exerts zero force on any ion, but this result is not a special case of (21b). Rather, (21b) should not be applied to the own sublattice, in which case the calculation should be different (and known to yield zero). However, (21c) gives correctly the force on the test ion from the other sublattice of the same atom layer. This force is always attractive and, for small ℓ , it is harmonic.

The functions $\Sigma_{s,d}(\ell)$ satisfy the following asymptotic relations:

$$\Sigma_s(\ell) \xrightarrow{\ell \rightarrow 0} 1/\ell^2, \quad (22a)$$

$$\Sigma_d(\ell) \xrightarrow{\ell \rightarrow 0} \pi b_1 \ell, \quad (22b)$$

$$\Sigma_{s,d}(\ell) \xrightarrow{\ell \rightarrow \infty} \pi, \quad (22c)$$

where $b_1 \approx 1.85885$. Also, $\Sigma_s(\ell) - \pi$ approaches zero exponentially fast when $\ell \rightarrow \infty$. Utilizing these observations, it is

convenient to write

$$\Sigma_s(\ell) = \pi + \frac{1}{\ell^2} S_s(\ell), \quad \Sigma_d(\ell) = \pi(1 - S_d(\ell)), \quad (23)$$

where the functions $S_{s,d}(\ell)$ satisfy

$$S_s(\ell) \xrightarrow{\ell \rightarrow 0} 1 - \pi \ell^2, \quad (24a)$$

$$S_d(\ell) \xrightarrow{\ell \rightarrow 0} 1 - b_1 \ell, \quad (24b)$$

$$S_{s,d}(\ell) \xrightarrow{\ell \rightarrow \infty} 0. \quad (24c)$$

It follows from (22c) that, at large distances, both functions $\mathcal{F}_{s,d}(z, z')$ approach the limit in which the discrete sublattice is replaced by a continuous surface charge density $\sigma = q/2h$. This limit is reached with good precision already for $\ell > 2$, as will be demonstrated below.

Evaluating the lattice sums similar to those in (21b) and (21c) is a formidable task. Following the original work of Ewald [22], elaborate methods have been developed for computing electric fields or potential in ionic lattices [23–25]. In this work, we make use of the power of modern computers and do not rely on analytical methods of summation. Rather, we compute the lattice sums numerically in an interval of ℓ where the functions $S_{s,d}(\ell)$ are substantially larger than zero and then fit the results to an *ad hoc* analytical formula with the correct asymptotes. This approach provides satisfactory precision and efficiency allowing us to use the functions $S_{s,d}(\ell)$ in iterative computations of the equilibrium.

Details of the numerical procedure are as follows. First, we evaluated the series (21b) and (21c) by truncated the summation according to the condition $|n|, |m| \leq n_{\max}$, where n_{\max} is a large integer. Summation was performed using high-precision arithmetic. Therefore, while the computed samples can depend on the truncation parameter n_{\max} , they are not affected by round-off errors. Results are shown in Fig. 4 for several values of n_{\max} . It can be seen that, in the interval $0 \leq \ell \leq 2$, the series is converged with good precision for $n_{\max} = 128\,000$. When $\ell > 2$, the computed data points still noticeably depend on n_{\max} , but are relatively small, i.e., $\lesssim 10^{-4}$. Accurate determination of $S_{s,d}(\ell)$ for $\ell > 2$ requires significantly larger values of n_{\max} , which is problematic from both the computational and physical points of view. For example, assuming the lattice unit of NaCl, which is 0.564 nm, the truncation parameter $n_{\max} = 128\,000$ corresponds to a sample with the lateral dimensions of 0.14 mm. Increasing n_{\max} further entails consideration of samples with macroscopic dimensions. This indicates that the functions $S_{s,d}(\ell)$ at large values of ℓ , while defined mathematically, can be affected by the edge effects in finite three-dimensional samples.

Therefore we use the data for $0 \leq \ell \leq 2$, which are known reliably, to approximate $S_{s,d}(\ell)$ by the analytical functions $S_{s,d}^{(\text{appr})}(\ell)$ defined as

$$S_s^{(\text{appr})}(\ell) = \frac{1 + (\lambda_s - a_1)\ell}{1 - a_1\ell + a_2\ell^2 - a_3\ell^3 + a_4\ell^4} e^{-\lambda_s \ell}, \quad (25a)$$

$$S_d^{(\text{appr})}(\ell) = \frac{1 + (\lambda_d - b_1)\ell + c_2\ell^2}{1 + b_2\ell^2 + b_3\ell^3 + b_4\ell^4} e^{-\lambda_d \ell}. \quad (25b)$$

Numerical values of the coefficients were obtained by the nonlinear fitting function implemented in Gnuplot and are listed in Table II. The constant b_1 is the same as in (22b). The

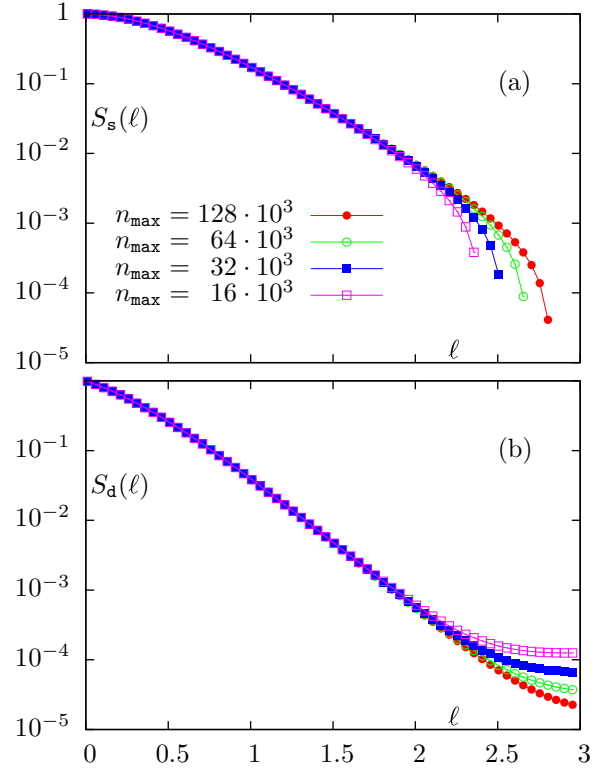


FIG. 4. Numerically computed functions $S_s(\ell)$ (a) and $S_d(\ell)$ (b) for different truncation parameters n_{\max} .

coefficients satisfy the constraint $a_2 - a_1\lambda_s + \lambda_s^2/2 \approx \pi$. Note that $S_{s,d}^{(\text{appr})}(\ell)$ satisfy the asymptotic relations (24). Quality of the fit is illustrated in Fig. 5.

We can now define the internal electrostatic force that acts on every ion. Let F_n^A and F_n^B be the electrostatic forces (projections onto the Z axis) acting on n th ion in chains A and B due to all other ions in the lattice (interaction with the external field will be introduced separately). We then have

$$F_n^A = \mathcal{F}_d(\xi_n^A, \xi_n^B) \text{sgn}(\xi_n^B - \xi_n^A) + \sum_{m \neq n} \text{sgn}(m - n) \times (-1)^{m-n} [\mathcal{F}_d(\xi_n^A, \xi_m^B) - \mathcal{F}_s(\xi_n^A, \xi_m^A)], \quad (26a)$$

$$F_n^B = \mathcal{F}_d(\xi_n^B, \xi_n^A) \text{sgn}(\xi_n^A - \xi_n^B) + \sum_{m \neq n} \text{sgn}(m - n) \times (-1)^{m-n} [\mathcal{F}_d(\xi_n^B, \xi_m^A) - \mathcal{F}_s(\xi_n^B, \xi_m^B)]. \quad (26b)$$

TABLE II. Numerical coefficients used in the analytical approximation (25) and in all simulations of this paper.

	c_2	λ_s	λ_d	
	1.47784	2.79038	3.90852	
k	1	2	3	4
a_k	0.609725	0.961619	0.366649	0.135
b_k	1.85885	1.09622	0.0821155	0.128119

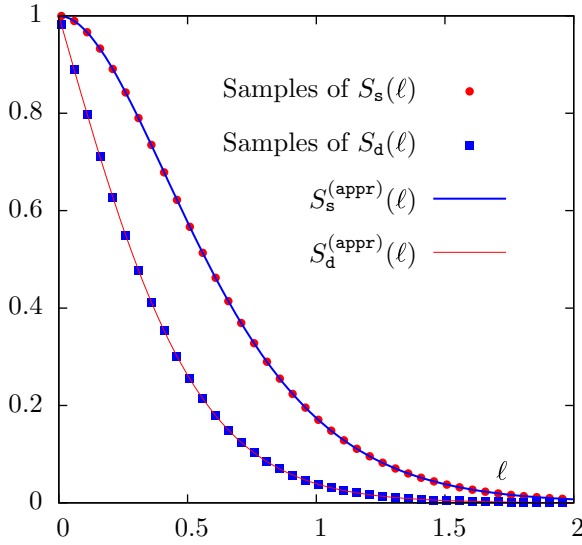


FIG. 5. Illustrating the quality of fit of $S_{s,d}(\ell)$ by the analytical approximations $S_{s,d}^{(\text{appr})}(\ell)$ (25).

Here the first terms in each expression describe interaction with the other sublayer of the same (n th) atom layer whereas the sum over m captures the interaction over all other atom layers in the structure. Using the expressions (21) and (VA), we can also write

$$F_n^A = \kappa \left\{ \pi [1 - S_d(|\xi_n^A - \xi_n^B|)] \text{sgn}(\xi_n^B - \xi_n^A) - \sum_{m \neq n} (-1)^{m-n} \text{sgn}(m-n) \times \left[\pi S_d(|\xi_n^A - \xi_m^B|) + \frac{S_s(|\xi_n^A - \xi_m^A|)}{|\xi_n^A - \xi_m^A|^2} \right] \right\}, \quad (27a)$$

$$F_n^B = \kappa \left\{ \pi [1 - S_d(|\xi_n^B - \xi_n^A|)] \text{sgn}(\xi_n^A - \xi_n^B) - \sum_{m \neq n} (-1)^{m-n} \text{sgn}(m-n) \times \left[\pi S_d(|\xi_n^B - \xi_m^A|) + \frac{S_s(|\xi_n^B - \xi_m^B|)}{|\xi_n^B - \xi_m^B|^2} \right] \right\}. \quad (27b)$$

Note that the above formulas rely on the assumption that $\xi_n^A, \xi_n^B < \xi_{n+1}^A, \xi_{n+1}^B$. Although one can envisage deformations of the lattice that violate this inequality, the structure becomes mechanically unstable at much smaller deformations and, in practice, we may assume that the above condition always holds. In the simulations, we use the expressions (27) to compute the internal electrostatic forces where $S_{s,d}(\ell)$ are approximated as (25) in the interval $0 \leq \ell \leq 2$ and taken to be zero for $\ell > 2$.

B. Elastic forces (chemical bonds)

The elastic forces can be decomposed into a sum of forces that originate from the bonds to other ions in the same chain

as the test ion (these forces are denoted by $L_n^{A,B}$ for the chains of the A or B type, respectively) and forces due to the lateral springs that connect each test ion to four neighboring ions of the same atom layer (these forces are denoted by $K_n^{A,B}$). We have

$$L_1^{A,B} = \xi_2^{A,B} - \xi_1^{A,B} - 1, \quad (28a)$$

$$L_n^{A,B} = \xi_{n-1}^{A,B} - 2\xi_n^{A,B} + \xi_{n+1}^{A,B}, \quad 1 < n < N; \quad (28b)$$

$$L_N^{A,B} = 1 + \xi_{N-1}^{A,B} - \xi_N^{A,B}. \quad (28c)$$

and

$$K_n^A = 4 \left(1 - \frac{1}{\sqrt{(\xi_n^B - \xi_n^A)^2 + 1}} \right) (\xi_n^B - \xi_n^A), \quad (28d)$$

$$K_n^B = 4 \left(1 - \frac{1}{\sqrt{(\xi_n^A - \xi_n^B)^2 + 1}} \right) (\xi_n^A - \xi_n^B). \quad (28e)$$

The expressions for $K_n^{A,B}$ are valid for all n including the surface layers, that is, for $1 \leq n \leq N$. Obviously, we have $K_n^A = -K_n^B$. For small deformations, we have $K_n^A = -K_n^B \approx 2(\xi_n^B - \xi_n^A)^3$. However, in the simulations, we use the exact formulas involving the square root.

C. External electric field and pressure

So far in this section, we considered only internal forces that are exerted by the ions on each other either by electrostatic or by elastic interactions. The model also involves external forces, which are produced by the applied electric field and externally applied pressure. While the applied electric field interacts with each ion in the lattice, the external pressure applies forces only on the boundary atom layers $n = 1$ and $n = N$.

Denote the total external force on an ion in n th layer and belonging to either A-type or B-type chain by $M_n^{A,B}$. Then

$$M_n^A = (\delta_{n1} - \delta_{nN}) p - (-1)^n \kappa e, \quad (29)$$

$$M_n^B = (\delta_{n1} - \delta_{nN}) p + (-1)^n \kappa e, \quad (30)$$

where p and e are dimensionless external pressure and electric field defined as the following ratios:

$$p = \Pi_{\text{ext}} h/k, \quad e = E_{\text{ext}} h^2/q. \quad (31)$$

Here Π_{ext} and E_{ext} are the applied pressure (not to be confused with the electrically induced pressure Π_{ind}) and the applied electric field in physical units.

VI. ITERATIVE COMPUTATION OF THE COORDINATES

In this section, we state the condition of equilibrium and introduce iterative algorithms for finding the ion coordinates at a given applied electric field and pressure. Since all chains of the same type are equivalent, the problem involves only $2N$ unknowns. However, finding these unknowns numerically is not an easy task. The equation of equilibrium is nonlinear and cannot be solved analytically while simple iterative schemes

possess numerical instabilities. This is why we go into considerable lengths to define stable and convergent numerical methods that can solve the problem, in particular, in the more difficult case when the applied field is not zero and the A and B chains are not equivalent.

A. Condition of equilibrium

The condition of equilibrium is that the net force acting on each ion is zero:

$$F_n^{A,B} + L_n^{A,B} + K_n^{A,B} + M_n^{A,B} = 0. \quad (32)$$

This equation must be solved with respect to the set of $2N$ coordinates, which we denote as

$$\{\xi\} = \{\xi_1^A, \xi_2^A, \dots, \xi_N^A, \xi_1^B, \xi_2^B, \dots, \xi_N^B\}. \quad (33)$$

Solving (32) analytically is of course an impossible task. We can however define an iterative scheme for computing the equilibrium set $\{\xi\}_{\text{eq}}$. To this end, we group separately the terms in (32) that are linear in $\{\xi\}$ and those that are nonlinear or independent of $\{\xi\}$. The elastic forces $L_n^{A,B}$ are always linear, and therefore they go into the first group. An additional linear contribution is hidden in the electrostatic forces $F_n^{A,B}$, specifically, in the first term in the figure brackets of (27). If this contribution is not properly grouped with $L_n^{A,B}$, the resulting iterations would be unstable. To obtain the required linearization, we recall the asymptotic formula (24b) for $S_d(\ell)$. This asymptote implies that, at small separations, the interaction of two sublayers of the same atom layer is harmonic; it is this harmonic attraction that helps stabilize the iterations. We therefore rewrite (27) as

$$F_n^A = \pi b_1 \kappa (\xi_n^B - \xi_n^A) + \tilde{F}_n^A, \quad (34a)$$

$$F_n^B = \pi b_1 \kappa (\xi_n^A - \xi_n^B) + \tilde{F}_n^B, \quad (34b)$$

where $\tilde{F}_n^{A,B}$ are given by the same expressions as in (27) except that, in the first term in the figure brackets, we must replace $[1 - S_d(|\xi_n^{A,B} - \xi_n^{B,A}|)]$ with $\tilde{S}_d(|\xi_n^{A,B} - \xi_n^{B,A}|)$, where

$$\tilde{S}_d(\ell) = 1 - b_1 \ell - S_d(\ell). \quad (35)$$

Note that

$$\tilde{S}_d(\ell) \xrightarrow{\ell \rightarrow 0} (b_2 - c_2 - \lambda_d b_1 + \lambda_d^2/2)\ell^2. \quad (36)$$

Numerical values of all constants are listed in Table II.

Given the above development, we can group all nonlinear terms as follows:

$$T_n^{A,B} = -(\tilde{F}_n^{A,B} + K_n^{A,B} + M_n^{A,B}). \quad (37)$$

For economy of space, we introduce a new constant

$$\beta = \pi b_1 \kappa. \quad (38)$$

It should be kept in mind that β is proportional to the model parameter κ . Then we write the linear terms explicitly and obtain the following stability condition:

$$n = 1 : \quad \xi_2^A - \xi_1^A - 1 + \beta(\xi_1^B - \xi_1^A) = T_1^A[\{\xi\}], \quad (39a)$$

$$\xi_2^B - \xi_1^B - 1 + \beta(\xi_1^A - \xi_1^B) = T_1^B[\{\xi\}], \quad (39b)$$

$1 < n < N :$

$$\xi_{n-1}^A - 2\xi_n^A + \xi_{n+1}^A + \beta(\xi_n^B - \xi_n^A) = T_n^A[\{\xi\}], \quad (39c)$$

$$\xi_{n-1}^B - 2\xi_n^B + \xi_{n+1}^B + \beta(\xi_n^A - \xi_n^B) = T_n^B[\{\xi\}], \quad (39d)$$

$n = N :$

$$1 + \xi_{N-1}^A - \xi_N^A + \beta(\xi_N^B - \xi_N^A) = T_N^A[\{\xi\}], \quad (39e)$$

$$1 + \xi_{N-1}^B - \xi_N^B + \beta(\xi_N^A - \xi_N^B) = T_N^B[\{\xi\}]. \quad (39f)$$

Note that, for small lattice distortions $T_n^{A,B}[\{\xi\}] = M_n^{A,B} + O(\{\xi\}^2)$.

The system of equation (39) is the starting point of all iterations. However, the iterations are run differently depending on whether the applied electric field is zero or not. Even if the applied field is not zero, we first run the iterations to determine $\{\xi\}_{\text{eq}}$ for given external pressure and zero external field; this result is then used as the initial guess for nonzero applied field. If this sequence is not followed, numerical instabilities may arise. Therefore we describe below the algorithms for zero and nonzero applied fields separately.

B. Algorithms for zero applied field

In the case $e = 0$, the A-type and B-type chains are equivalent and we can write $\xi_n^A = \xi_n^B = \xi_n$ and $T_n^A = T_n^B = T_n$. Equations (39) simplify as

$$\xi_2 - \xi_1 - 1 = T_1[\{\xi\}], \quad (40a)$$

$$\xi_{n-1} - 2\xi_n + \xi_{n+1} = T_n[\{\xi\}], \quad 1 < n < N, \quad (40b)$$

$$1 + \xi_{N-1} - \xi_N = T_N[\{\xi\}]. \quad (40c)$$

The left-hand side defines a simple three-point recursion. Due to translational invariance of all physical properties, we can set without loss of generality the initial guess to be $(\xi_n)_0 = n - 1$ and then, for $i = 1, 2, \dots$, define the recursive step as

$$(\xi_1)_{i+1} = 0, \quad (41a)$$

$$(\xi_2)_{i+1} = 1 + T_1[\{\xi\}]_i \quad (41b)$$

$$(\xi_n)_{i+1} = 2(\xi_{n-1})_i - (\xi_{n-2})_i + T_{n-1}[\{\xi\}]_i, \quad (41c)$$

for $3 \leq n \leq N$.

It can be seen that the force $T_N[\{\xi\}]_i$ does not appear in (41). However, it can be used in a consistency check, which is of the form

$$1 + (\xi_{N-1})_{i+1} - (\xi_N)_{i+1} + T_N[\{\xi\}]_i = 0. \quad (42)$$

Assuming the consistency check is successful with some predetermined precision, we repeat the iteration step (41) until the stop condition $\|\{\xi\}_{i+1} - \{\xi\}_i\|_2 \leq \varepsilon$ is met, where ε is some small predetermined constant and $\|\cdot\|_2$ is the L_2 norm. Note that computation of $T_n[\{\xi\}]_i$ is simplified in the absence of applied field. In particular, we have $K_n^{A,B} = 0$ (lateral springs do not exert any force). Also, in (34), $F_n^A = F_n^B = F_n$, the first term (proportional to $\pi b_1 \kappa$) is zero and, in the expression for \tilde{F}_n , we have $\tilde{S}_d(|\xi_n^{A,B} - \xi_n^{B,A}|) = 0$.

Algorithm 1. Computing equilibrium coordinates for zero applied field.

Require: Input parameters $N, p, \kappa; e = 0$.

- 1: Initialize $0 < \varepsilon \ll 1, i = 0$ and $i_{\max} \gg 1$
- 2: Initialize $\{\xi\}$ as $\xi_n \leftarrow n - 1$ for $1 \leq n \leq N$
- 3: Initialize $\{\xi\}_{\text{old}} \leftarrow \{\xi\}$
- 4: **loop**
- 5: $i \leftarrow i + 1$
- 6: **If** $i > i_{\max}$ **then**
- 7: **return** error ▷ Max num. iter. exceeded; stop
- 8: **end if**
- 9: **for** $n = 1$ to N **do**
- 10: $t_n \leftarrow T_n[\{\xi\}]$
- 11: **end for**
- 12: $\xi_1 \leftarrow 0; \xi_2 \leftarrow 1 + t_1$
- 13: **for** $n = 3$ to N **do**
- 14: $\xi_n \leftarrow 2\xi_{n-1} - \xi_{n-2} + t_{n-1}$
- 15: **end for**
- 16: $\delta \leftarrow |1 + \xi_{N-1} - \xi_N + t_N|$
- 17: **if** $\delta > \varepsilon$ **then**
- 18: **return** error ▷ Consistency test failed; stop
- 19: **end if**
- 20: test $\leftarrow \|\{\xi\} - \{\xi\}_{\text{old}}\|_2$
- 21: **if** test $> \varepsilon$ **then**
- 22: $\{\xi\}_{\text{old}} \leftarrow \{\xi\}$ ▷ Continue iterations
- 23: **else**
- 24: **return** $\{\xi\}_{\text{eq}} \leftarrow \{\xi\}$ ▷ All ions at equilibrium
- 25: **end if**
- 26: **end Loop**

We can now define an algorithm for computing ξ_n at $e = 0$. The corresponding pseudocode is given in Algorithm 1. Note that, in the $(i + 1)$ th iteration, we use the vector $T_n[\{\xi\}_i]$ that was computed right after the i th iteration (in lines 9–11). The forces $T_n[\{\xi\}_i]$ are not updated in lines 12–15. Algorithm 1 is stable and convergent. The stop condition test $\leq \varepsilon$ (lines 20–25) is met at a modest number of iterations. Consequently, the stop condition based on the number of iterations (lines 6–8) is typically not used. Convergence can be achieved at or close to the machine precision, but selecting $\varepsilon = 10^{-8}$ is sufficient in practice.

C. Algorithm for nonzero applied field

In Algorithm 1, we make a complete iterative step updating the coordinates $\{\xi\}$ of a complete chain using the nonlinear forces $T_n[\{\xi\}]$ determined at the previous iteration. This approach will not work in the case of nonzero applied field. The main reason is that the A-type and B-type chains are no longer equivalent in this case. The applied field tries to extend one chain and contract the other. If we solve the three-point recursion for each chain separately, the resulting chains would be of different lengths. Even if the *relative* difference of the lengths of A-type and B-type chains is small, the *absolute* difference can become comparable or larger than h . Obviously, such an intermediate solution is far away from the equilibrium. Updating the nonlinear forces and repeating the iteration will result in runaway oscillations and, eventually, will violate the basic assumption $\xi_n^A, \xi_n^B < \xi_{n+1}^A, \xi_{n+1}^B$ under

which the electrostatic forces are computed. We will therefore proceed by updating the coordinates of one atom layer at a time.

Still, (39) is too complicated to be solved efficiently by iterations. The linearized left-hand side is no longer a simple three-point recursion and it cannot be analytically inverted. The left-hand side of (39) can be viewed as a matrix-vector product where an $2N \times 2N$ matrix A acts on the vector $\{\xi\}$. This matrix can be, in principle, inverted to yield a recursion generator of the form $\{\xi\} = A^{-1}T[\{\xi\}]$. However, a more computationally efficient and stable approach is to seek equilibrium of one atom layer at a time while updating the nonlinear forces after each update of the coordinates. To this end, we make one additional (identical) transformation of (39). Viewing each line of this set as a linear equation for ξ_n^A and ξ_n^B , moving all other terms to the right-hand side, we obtain

$$\begin{aligned} \xi_1^A &= \frac{\beta}{1 + 2\beta} (\xi_2^B - 1 - T_1^B[\{\xi\}]) \\ &+ \frac{1 + \beta}{1 + 2\beta} (\xi_2^A - 1 - T_1^A[\{\xi\}]) \equiv R_1^A[\{\xi\}], \end{aligned} \quad (43a)$$

$$\begin{aligned} \xi_1^B &= \frac{\beta}{1 + 2\beta} (\xi_2^A - 1 - T_1^A[\{\xi\}]) \\ &+ \frac{1 + \beta}{1 + 2\beta} (\xi_2^B - 1 - T_1^B[\{\xi\}]) \equiv R_1^B[\{\xi\}], \end{aligned} \quad (43b)$$

$$\begin{aligned} \xi_n^A &= \frac{\beta}{4(1 + \beta)} (\xi_{n-1}^B + \xi_{n+1}^B - T_n^B[\{\xi\}]) \\ &+ \frac{2 + \beta}{4(1 + \beta)} (\xi_{n-1}^A + \xi_{n+1}^A - T_n^A[\{\xi\}]) \equiv R_n^A[\{\xi\}], \end{aligned} \quad (43c)$$

$$\begin{aligned} \xi_n^B &= \frac{\beta}{4(1 + \beta)} (\xi_{n-1}^A + \xi_{n+1}^A - T_n^A[\{\xi\}]) \\ &+ \frac{2 + \beta}{4(1 + \beta)} (\xi_{n-1}^B + \xi_{n+1}^B - T_n^B[\{\xi\}]) \equiv R_n^B[\{\xi\}], \end{aligned} \quad (43d)$$

$$\begin{aligned} \xi_N^A &= \frac{\beta}{1 + 2\beta} (\xi_{N-1}^B + 1 - T_N^B[\{\xi\}]) \\ &+ \frac{1 + \beta}{1 + 2\beta} (\xi_{N-1}^A + 1 - T_N^A[\{\xi\}]) \equiv R_N^A[\{\xi\}], \end{aligned} \quad (43e)$$

$$\begin{aligned} \xi_N^B &= \frac{\beta}{1 + 2\beta} (\xi_{N-1}^A + 1 - T_N^A[\{\xi\}]) \\ &+ \frac{1 + \beta}{1 + 2\beta} (\xi_{N-1}^B + 1 - T_N^B[\{\xi\}]) \equiv R_N^B[\{\xi\}]. \end{aligned} \quad (43f)$$

This can be rewritten succinctly as

$$\xi_n^{A,B} = R_n^{A,B}[\{\xi\}], \quad (44)$$

where $R_n^{A,B}[\{\xi\}]$ are defined in right-hand sides of (43). We emphasize that (44) is not an approximation but an identical transformation of (39). The advantage of (44) is that it can be iterated for each atom layer until it reaches an equilibrium given the coordinates of all other layers (which may not yet be at equilibrium). We then cycle over all layers until the equilibrium is found.

Algorithm 2. Computing equilibrium coordinates for nonzero applied field.

Require: Input parameters N, p, e, κ
Require: Use Algorithm 1 with $e = 0$ (alternatively, use Algorithm 2 with previous, smaller value of e) to compute the initial guess $\{\xi\}_0$

- 1: Initialize $0 < \varepsilon_1, \varepsilon_2 \ll 1$, and $i_{\max}, j_{\max} \gg 1$
- 2: Initialize $\{\xi\} \leftarrow \{\xi\}_0; \{\xi\}_{\text{old}} \leftarrow \{\xi\}; i = 0$
- 3: **loop** L1
- 4: $i \leftarrow i + 1$
- 5: **if** $i > i_{\max}$ **then**
- 6: **return** error ▷ Max iter. exceeded
- 7: **end if**
- 8: **for** $n = 1$ to N **do** ▷ Loop over atom layers
- 9: $\zeta_n^A \leftarrow \xi_n^A; \zeta_n^B \leftarrow \xi_n^B; j = 0$
- 10: **loop** L2 (for layer n)
- 11: $j \leftarrow j + 1$
- 12: **if** $j > j_{\max}$ **then**
- 13: **return** error ▷ Max iter. exceeded
- 14: **end if**
- 15: $\xi_n^A \leftarrow R_n^A[\{\xi\}]; \xi_n^B \leftarrow R_n^B[\{\xi\}]$
- 16: test $\leftarrow \sqrt{(\xi_n^A - \zeta_n^A)^2 + (\xi_n^B - \zeta_n^B)^2}$
- 17: **if** test $\leq \varepsilon_1$ **then**
- 18: Exit Loop L2 (n th layer at equilibrium)
- 19: **else**
- 20: $\zeta_n^A \leftarrow \xi_n^A; \zeta_n^B \leftarrow \xi_n^B$ ▷ Continue iterations
- 21: **end if**
- 22: **end loop** L2
- 23: **end for**
- 24: test $\leftarrow \|\{\xi\} - \{\xi\}_{\text{old}}\|_2$
- 25: **if** test $\leq \varepsilon_2$ **then**
- 26: **return** $\{\xi\}_{\text{eq}} \leftarrow \{\xi\}$ ▷ All ions at equilibrium
- 27: **else**
- 28: $\{\xi\}_{\text{old}} \leftarrow \{\xi\}$ ▷ Continue iterations
- 29: **end if**
- 30: **end loop** L1

These ideas give rise to Algorithm 2. Here we utilize the equilibrium positions obtained by Algorithm 1 (alternatively, from Algorithm (2) for a previously used, smaller value of e , i.e., in a scan over e) as the initial guess. Importantly, the term $R_n^{A,B}[\{\xi\}]$ in line 15 is updated before the assignment operation using the current values of all coordinates $\{\xi\}$. This is different from Algorithm 1 and more computationally demanding but helps maintain stability. Note that the translational invariance along Z is not explicitly used in Algorithm 2. This is so because we start with a given initial guess and adjust each layer to its equilibrium one-by-one. For this reason, Algorithm 2 does not have or need a consistency check. The manifestation of translational invariance (which is, of course, present in the model) is that the obtained solutions are shifted along Z by Δ if we shift the initial guess by Δ , but the physical properties of the structure are invariant to this shift. Algorithm 2 is stable and convergent; selecting $\varepsilon_1 = \varepsilon_2 = 10^{-8}$ typically results in a reasonable run time and high precision of the obtained solutions. However, computing strain to high precision at relatively small values of e (first few data points in Fig. 12 below) may require $\varepsilon_1 = \varepsilon_2 = 10^{-12}$. Computations run in seconds to a minute per one value of

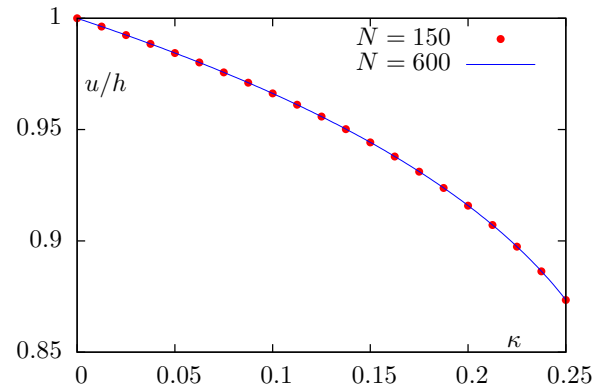


FIG. 6. Lattice unit in Z direction, u , computed according to (45a) as a function of the model parameter κ . At $\kappa = 0$ (no electrostatic interaction), $u = h$ both theoretically and numerically. The dots for $N = 150$ represent data points. The line for $N = 600$ connects data points that are sampled at a 10-times higher rate and therefore not shown explicitly.

e and $N = 150$, depending on the value of κ and required precision.

VII. PHYSICAL PROPERTIES

In this section, we compute the basic physical properties of the model. We will use the results of this section in Sec. VIII below to verify various theoretical predictions for the electrically induced pressure.

A. Lattice unit

As was mentioned in Sec. IV, the lattice unit of the model structure is fixed to h in the X and Y directions. However, in the Z direction, the attractive electrostatic interaction can reduce the interlayer separation. We denote by $\Lambda(p, e)$ the equilibrium width of the slab (in physical units) at applied dimensionless pressure p and dimensionless electric field e , which are defined in (31). Note that the slab width shown in Fig. 2 is $\Lambda_0 = \Lambda(0, 0)$. The lattice unit can be defined as either

$$u = \Lambda(0, 0)/(N - 1) \quad (45a)$$

or as

$$u = h(\xi_{N/2+1} - \xi_{N/2})|_{p=e=0}. \quad (45b)$$

Note that, at $e = 0$, $\xi_n^A = \xi_n^B = \xi_n$. The definition (45a) assumes that the atomic planes make a perfect lattice of step u . This is not quite so as the lattice cells close to the slab surfaces are different from those in the bulk. However, for $N = 150$, which is the number of layers for which most numerical results below have been obtained, the difference between the definitions (45a) and (45b) is negligible. We can say that the bulk limit has been reached at $N = 150$.

The lattice unit u has been computed by Algorithm 1 for various values of the model parameter κ . In Fig. 6, numerical results are shown for $N = 150$ atom layers (dots) and verified for $N = 600$ (line). As expected, $u \rightarrow h$ when $\kappa \rightarrow 0$. At $\kappa = 0.25$, we have $u \approx 0.87h$. If we increase κ further, the

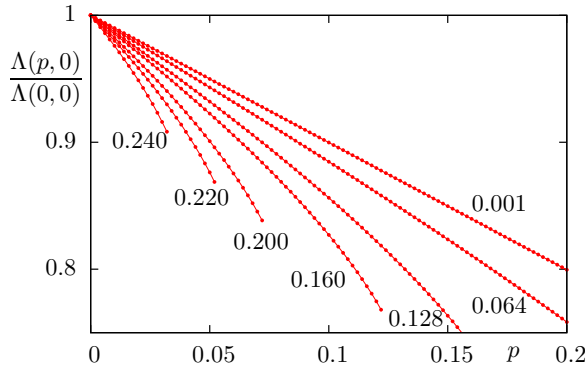


FIG. 7. Equilibrium width of the slab $\Lambda(p, 0)$ as a function of applied dimensionless pressure p for different model parameters κ (values labeled near each curve), $N = 150$ and $e = 0$. The function is normalized to the equilibrium width at $p = e = 0$, $\Lambda(0, 0) = (N - 1)u$, where the lattice unit u is shown in Fig. 6. Dots show the computed data points and lines are drawn to guide the eye.

system would lose mechanical stability as the electrostatic attraction overcomes the elastic repulsion. This is an artifact the simplistic assumption that the elastic forces remain harmonic regardless of the inter-ion distance. The assumption can be fixed in future refinements of the model by including additional nonlinear terms in $K_n^{A,B}$ to account for more realistic inter-ionic potentials. In this paper, we limit consideration to $\kappa \leq 0.25$.

B. Young's modulus

We next study the equilibrium width of the slab under applied external pressure and zero applied field, $\Lambda(p, 0)$. We apply the external pressure to both surfaces of the slab, so that the total force is zero. As $e = 0$, we can still use Algorithm 1 for the computations. Figure 7 shows the ratio $\Lambda(p, 0)/\Lambda(0, 0)$ as a function of the dimensionless pressure p for several values of the model parameter κ . Each curve is plotted up to the critical pressure above which the structure collapses. Obviously, the critical pressure becomes smaller when κ is increased.

Young's modulus η can be computed from the slopes of the curves shown in Fig. 7 near the point $p = 0$. The definition (for the dimensionless combination $h\eta/k$) is

$$\frac{h\eta}{k} = - \left[\frac{\partial}{\partial p} \frac{\Lambda(p, 0)}{\Lambda(0, 0)} \Big|_{p=0} \right]^{-1} \approx \frac{\delta p \Lambda(0, 0)}{\Lambda(0, 0) - \Lambda(\delta p, 0)}, \quad (46)$$

where δp is a small increment of the dimensionless pressure. Note that, at $\kappa = 0$, the derivative in square brackets is equal to -1 and the corresponding theoretical limit is $\eta(\kappa = 0) = k/h$. This is, approximately, the case for the curve with $\kappa = 0.001$ in Fig. 7. As we increase κ , η is expected to decrease. This is illustrated in Fig. 8 where we plot $h\eta/k$ as a function of κ . We have computed the derivative in (46) using $\delta p = 0.001$. It can be seen that the lattice loses stiffness as κ is increased. For $\kappa > 0.25$, Young's modulus goes quickly to zero and the structure becomes mechanically unstable.

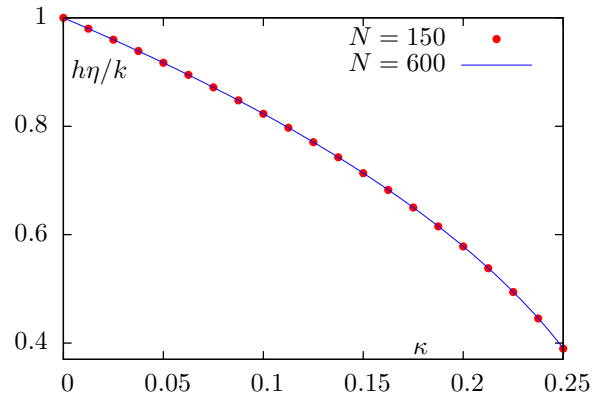


FIG. 8. Young's modulus η normalized to k/h (the theoretical value at $\kappa = 0$) as a function of κ . The dots for $N = 150$ represent data points. The line for $N = 600$ connects data points that are sampled at a 10-times higher rate and therefore not shown explicitly.

C. Dielectric permittivity

Defining dielectric permittivity in terms of dipole moment per unit volume is not always a robust approach [26,27], but in the physical model of this paper, this method can be used safely. The total dipole moments of the chains A and B are given by

$$d^A = -hq \sum_{n=1}^N (-1)^n \xi_n^A, \quad d^B = hq \sum_{n=1}^N (-1)^n \xi_n^B. \quad (47)$$

The volume per two neighboring chains is

$$V = h^3 (\xi_N^A - \xi_1^A + \xi_N^B - \xi_1^B). \quad (48)$$

In order to account for the electrically induced surface roughness, we have taken in (48) the width of the slab to be the average length of the chains A and B. However, in the bulk limit, the effect of surface roughness is minor. From (47) and (48), we find the electric polarization along Z as

$$P_z = \frac{d^A + d^B}{V} = E_{\text{at}} \frac{\sum_{n=1}^N (-1)^n (\xi_n^B - \xi_n^A)}{\xi_N^A - \xi_1^A + \xi_N^B - \xi_1^B}, \quad (49a)$$

where $E_{\text{at}} = q/h^2$ is the atomic field. On the other hand, polarization of a homogeneous slab in the geometry of Fig. 2 is

$$P_z = \frac{\epsilon - 1}{4\pi \epsilon} E_{\text{ext}}, \quad (49b)$$

where ϵ is the dielectric permittivity. Comparing (49a) and (49b) and recalling the definition $e = E_{\text{ext}}/E_{\text{at}}$, we find the expression for ϵ ,

$$\epsilon = \frac{1}{1 - 4\pi \mathcal{D}_0}, \quad (50a)$$

where

$$\mathcal{D}_0 = \frac{\partial \mathcal{D}}{\partial e} \Big|_{e=0} \approx \frac{\delta \mathcal{D}}{\delta e} \quad (50b)$$

and

$$\mathcal{D} = \frac{\sum_{n=1}^N (-1)^n (\xi_n^B - \xi_n^A)}{\xi_N^A - \xi_1^A + \xi_N^B - \xi_1^B}. \quad (50c)$$

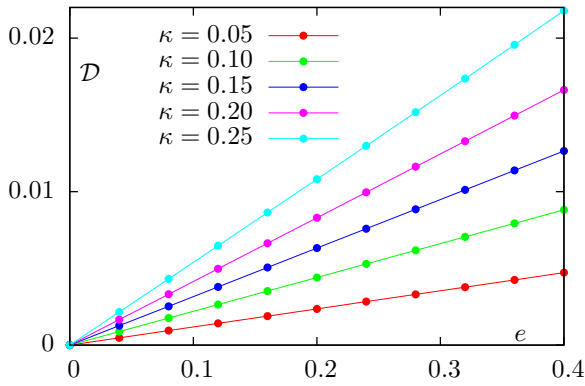


FIG. 9. Dimensionless dipole moment \mathcal{D} as a function of dimensionless applied field e for different values of the model parameter κ for $N = 150$. Every tenth computed data point is shown as a dot.

Here $\delta\mathcal{D}$ is the value of \mathcal{D} at a small increment δe of the dimensionless electric field. We have implicitly assumed that, at small e , $\mathcal{D} \approx \mathcal{D}_0 e$ with $\mathcal{D}_0 \neq 0$ (the first derivative does not vanish at $e = 0$), which indeed follows from symmetry since \mathcal{D} must change sign when e changes sign.

Computation of \mathcal{D} requires the use of Algorithm 2 as now we must take $e \neq 0$. This is somewhat slower than using Algorithm 1 but runs in seconds per a data point in the most challenging cases of relatively large κ and e and $N = 150$. In Fig. 9, we plot \mathcal{D} as a function of e in the interval $0 \leq e \leq 0.4$. It can be seen that \mathcal{D} is an approximately linear function of e in a wide range of parameters. The dielectric permittivity ϵ is determined by the slopes of the lines shown in Fig. 9 near the point $e = 0$, although this slope stays nearly constant in the whole range of e considered (small deviations from linearity exist but are not visually discernible from the figure).

We now have everything we need to compute the dielectric permittivity. We have evaluated the derivative in (50b) using $\delta e = 0.02$. The results are shown in Fig. 10 for $N = 150$ and $N = 600$. It can be seen that the dielectric permittivity is more sensitive to the number of atom layers N than the purely

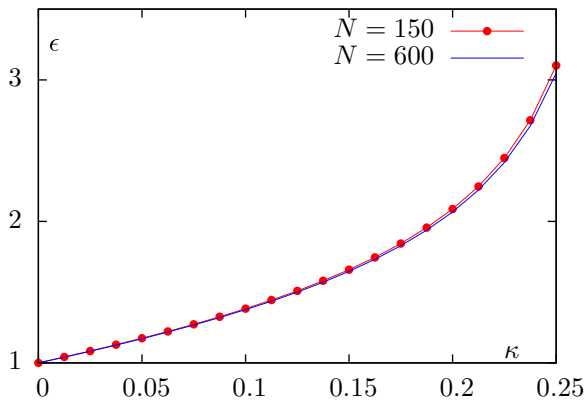


FIG. 10. Dielectric permittivity of the model structure as a function of κ at zero external pressure. Dots show every tenth computed data point for $N = 150$. Continuous connects all computed data points for $N = 600$.

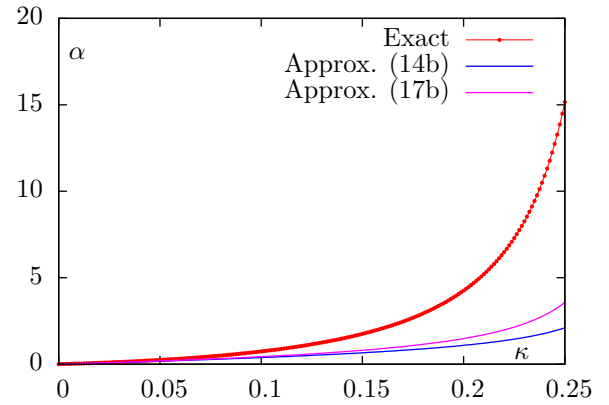


FIG. 11. Electrostrictive coefficient α as a function of κ for $N = 150$. For comparison, approximations (14b) and (17b) are also plotted where the data of Fig. 10 for ϵ have been used. Approximations are inaccurate for $\kappa \gtrsim 0.02$.

mechanical properties: there is a small but visible difference between the cases $N = 150$ and 600 . Increasing N even further (i.e., to $N = 1200$) does not change ϵ visibly but slows down the computations (data not shown). Considering that the difference between the $N = 150$ and 600 cases is already minor, we use $N = 150$ in the remainder of this paper.

It can also be commented that the maximum obtained value of ϵ (slightly larger than 3.0 at $\kappa = 0.25$) is still significantly smaller than the static dielectric constant of NaCl (between 4.0 and 5.0). However, in physical NaCl crystals, polarization occurs due to both lattice distortion and perturbation of the electron density. In the present model, we do not account for the electronic mechanism of polarization, and it could be expected that the obtained value of ϵ is underestimated.

D. Electrostrictive coefficient

We can compute the electrostrictive coefficient α by computing the change of ϵ due to externally applied pressure. The dielectric constant shown in Fig. 10 was computed at zero external pressure. Now let us increase the dimensionless pressure from 0 to δp and let the corresponding changes of the slab width and dielectric constant be $\delta\Lambda$ and $\delta\epsilon$. Obviously, $\delta\Lambda$ is negative and $\delta\epsilon$ is positive. We can compute the coefficients of interest using the relation

$$\alpha = -\Lambda_0 \frac{\delta\epsilon}{\delta\Lambda}. \quad (51)$$

Note that α is dimensionless. Also, $\Lambda_0 = \Lambda(0, 0)$ is the equilibrium slab width at zero applied pressure and zero applied electric field.

The coefficient α computed by Algorithm 2 according to (51) is plotted in Fig. 11 as a function of κ . We have used the increment of pressure $\delta p = 0.001$, which provides good accuracy (at least, three significant figures). The increment of the dimensionless electric field used to compute ϵ according to (50b) at both values of external pressure ($p = 0$ and $p = \delta p$) was $e = 0.02$. For comparison, we have also plotted the approximations (14b) and (17b). It can be seen that both approximations are inaccurate for $\kappa \gtrsim 0.02$.

TABLE III. Numerical values of the dimensionless Young's modulus $h\eta/k$, dielectric permittivity ϵ , the coefficient α appearing in the electrostriction force (11), and forms and numerical values of the function $g(\epsilon, \alpha)$ that correspond to the competing expressions for the force density (compare to Table I). All numbers are rounded off to four significant figures. Symbol H corresponds to the Helmholtz force density (13). All physical parameters displayed in this table are also shown in various plots of Sec. VII and have been computed for $N = 150$.

κ	$h\eta/k$	ϵ	α	$g(\epsilon, \alpha)$				
				(a) $-\frac{\epsilon^2 - 1}{\epsilon^2}$	(b) and (d) $-\frac{(\epsilon - 1)^2}{\epsilon^2}$	(c) $-\frac{\epsilon - 1}{\epsilon}$	elstr $\frac{\alpha}{\epsilon^2}$	H $\frac{\alpha - \epsilon(\epsilon - 1)}{\epsilon^2}$
0.05	0.9170	1.174	0.2451	0.2746	0.02198	0.1483	-0.1778	-0.02955
0.1	0.8231	1.383	0.7374	0.4771	0.07668	0.2769	-0.3855	-0.1086
0.2	0.5782	2.088	4.254	0.7706	0.2714	0.5210	-0.9760	-0.4550

In particular, the Clausius-Mossotti approximation does not work well in the model considered here.

VIII. ELECTRICALLY INDUCED STRAIN

In this section, we present the central result of this paper. We now consider the case when the applied electric field is varied at zero external pressure. Even though we apply no external mechanical pressure, the applied electric field is expected to produce strain in the slab, which we denote by $\sigma(e)$,

$$\sigma(e) = \Lambda(0, e)/\Lambda(0, 0) - 1. \quad (52a)$$

We interpret this strain as being caused by the electrically induced pressure $\Pi_{\text{ind}}(e)$ according to

$$\sigma(e) = -\frac{1}{\eta} \Pi_{\text{ind}}(e), \quad (52b)$$

where η is Young's modulus whose value is displayed in Fig. 8 as a function of the model parameter κ . Note that, according to the convention, positive surface pressure induces negative strain (compression) and *vice versa*. Various theoretical expressions for $\Pi_{\text{ind}}(e)$ corresponding to the competing expressions for the electrostatic force density are summarized in Table I. It follows from Table I and (52b) that the theoretical relationship between $\sigma(e)$ and e is of the form

$$\sigma(e) = \frac{\kappa g(\epsilon, \alpha)}{8\pi(h\eta/k)} e^2, \quad (53)$$

where $g(\epsilon, \alpha)$ is a dimensionless function whose form depends on the theoretical expression for $\Pi_{\text{ind}}(e)$. Obviously, the physical parameters η , α and ϵ depend on κ as is illustrated in Figs. 8, 10, and 11. Below, we compute the electrically induced strain numerically for the following three values of κ : 0.05, 0.1, and 0.2. Table III summarizes numerical values of the corresponding physical parameters as well as the theoretical forms and numerical values of $g(\epsilon, \alpha)$.

The electrically induced strain $\sigma(e)$ (52a) was computed by Algorithm 2, where we have defined $\Lambda(0, e)$ as the average of the lengths of A and B chains. In Fig. 12, we plot $\sigma(e)$ for the three values of κ shown in Table III and compare the results to various theoretical predictions. It can be seen that $\sigma(e)$ is quadratic in e (as one could expect from symmetry) and much smaller in magnitude than the strain that can be induced by external pressure at comparable values of the dimensionless external pressure and field, $p \sim e$. Although all theoretical

predictions for the strain are not orders of magnitude apart, the Helmholtz force density is clearly the winner and, in fact, yields remarkably accurate predictions.

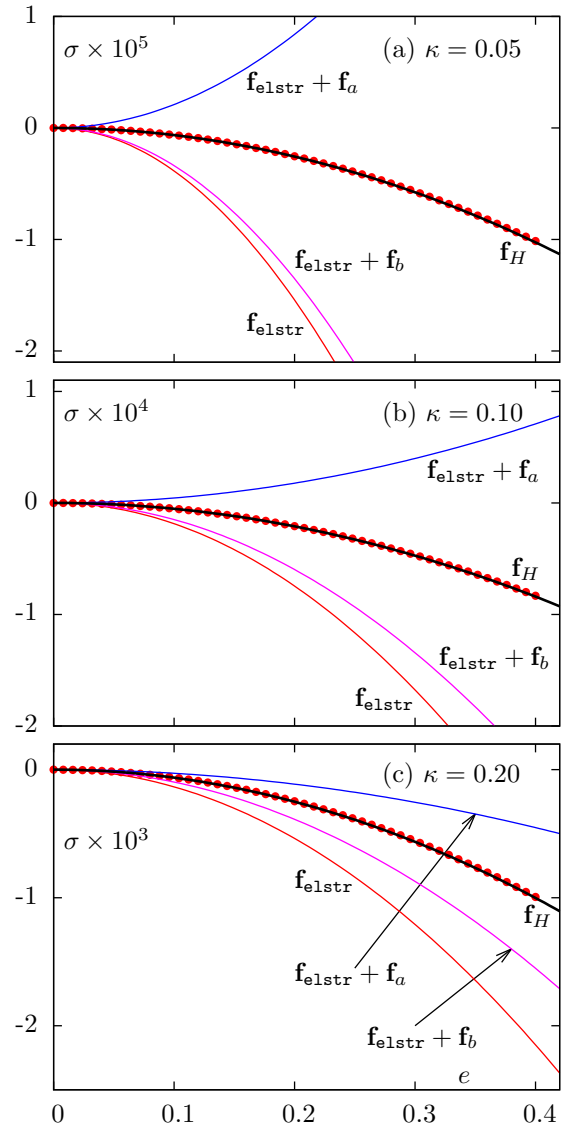


FIG. 12. Comparison of numerically computed electrically induced strain $\sigma(e)$ (52a) (points) and various theoretical predictions (lines) for $\kappa = 0.05$ (a), 0.1 (b), and 0.2 (c), as functions of the dimensionless applied field $e = h^2 E_{\text{ext}}/q$. $N = 150$.

We now discuss the data of Fig. 12 in more detail. First, at all three values of κ considered, we have $\sigma(e) < 0$. This corresponds to compression of the slab. We can conclude that the expansion forces $\mathbf{f}_a(\mathbf{r})$, $\mathbf{f}_b(\mathbf{r}) = \mathbf{f}_d(\mathbf{r})$ and $\mathbf{f}_c(\mathbf{r})$ cannot adequately describe elastic deformation of the slab. However, the electrostriction force alone strongly overestimates the effect. We must therefore add the electrostriction force to one of the expansion forces to obtain the correct prediction. It can be seen that adding together $\mathbf{f}_{\text{elstr}}(\mathbf{r})$ with $\mathbf{f}_c(\mathbf{r})$, which results in the Helmholtz force density according to (13), yields an accurate precision in all considered cases.

Second, the approximations (14b) and (17b) for the coefficient α are both inaccurate. In fact, using these approximations for α in the Helmholtz force density would still predict positive strain (expansion rather than contraction). It can be concluded that the Clausius-Mossotti approximation is not accurate for ionic crystals.

Finally, it should be emphasized that the results of Fig. 12 are not circular. We did not use any of the previously computed physical parameters (η , ϵ , α) to compute the strain $\sigma(e)$. Rather, we have used these quantities in the theoretical predictions for $\sigma(e)$. The remarkable accuracy of the Helmholtz force density is not an artifact but a consequence of the deep physical insight of the underlying theory.

IX. DISCUSSION

Following the original work of Helmholtz [7], electrostatic forces in dielectrics are often considered macroscopically from very general first principles of thermodynamics and energy conservation [[17], §15]. However, the electrostriction forces can also be understood microscopically as consequences of anharmonicity of ionic interactions [28]. The anharmonicity-based argument can be readily understood from the schematics of Fig. 3. In a nonpolarized lattice, there is a force of attraction between adjacent atom layers, which ultimately establishes the lattice unit u (displayed in Fig. 6 above). When we apply external electric field, the ions shift from their positions. Considering two adjacent layers, we see that some pairs of oppositely charged ions move closer to each other (in the direction parallel to the applied field) and some move further apart. If the interion potential was ideally harmonic, the overall force of attraction between the two layers would not change. But due to the anharmonicity, the increase in the attraction between the ions that move closer is not compensated by the decrease in attraction between the two ions that move further apart. As a result, the overall force of attraction between two adjacent layers is increased, which results in a smaller lattice unit—an effect that can be interpreted as electrically induced strain.

As is often the case, the macroscopic and microscopic theories cannot be easily derived from each other. The proposed model provides a bridge between these two descriptions. An interesting feature of this model is that it is purely classical yet captures the essential physics correctly. Quantum description based on the density-functional theory is more fundamental but leads to substantial complexity, especially, when boundaries are introduced. However, accounting for boundaries and finite size of the objects is essential for understanding the

electrically induced forces. The model of this paper allows one to consider boundaries with relative ease.

While simulations reported above concern one-dimensional compression of a plane-parallel layer and a specific microstructure, it is hoped that the model can be extended to crystals of more general macroscopic and microscopic geometry. Considering macroscopic samples that are finite in all three dimensions will create more complicated strain and stress. This will also allow one to account quantitatively for the fact that different lattice cells (near the corners, edges, flat surfaces or in the bulk) have different geometrical and physical properties. The associated effects can influence the macroscopic properties of crystals, including stability conditions, which determine which kinds of surfaces are possible (the generalized Tasker condition) and also bulk polarization [19]. The model can also be extended to different and more complicated microstructures. The author believes that the accuracy of the Helmholtz formula is not an artifact of the specific crystal structure of NaCl but will persist for other crystals, in particular, for those with more than two different ions. It is also possible to introduce phenomenologically electronic polarization into the model. Some more generally applicable theoretical formulas for the force density are given in Appendix. The Helmholtz force density is expected to remain accurate at least in statics and in linear systems with a center of symmetry (in noncentrosymmetric crystals, we also need to account for the piezoelectric effect, which is typically much stronger). However, verification of these prediction requires additional simulations.

The model developed in this paper can be viewed as a generalization of the Lorentz model of molecular polarization to a macroscopic crystal. While the Lorentz model can be easily solved analytically, the model of this paper requires numerical simulations. Another difference is that the Lorentz model concerns a pointlike object (a molecule) and therefore can describe effects such as electric polarization, radiation and scattering. The model of this paper describes an extended object and can, in addition, capture electro-mechanical effects such as electrostriction. For a different crystal geometry, the model can also become applicable to the piezoelectric effect, which is linear in the applied field and absent in crystals with a center of symmetry such as NaCl. We also hope that the model can be generalized beyond statics and used in the dynamic theory of electrostriction, which is a topic of current interest [29].

The numerical methods developed in this paper are based on seeking the zero of force rather than the minimum of potential. The two methods are related as force is the gradient of the potential. Both algorithms described in Sec. VI are some forms of descent although we do not prove that the descent is steepest and do not seek the global minimum. In fact, the total potential of the model has many singularities (when two ions of opposite charge coalesce) and the total potential energy is not a convex function of the ionic coordinates. Instead of searching for a unique global minimum (which we know does not exist), we seek the local minimum that is not too far from the unperturbed configuration and satisfies some consistency conditions such as $\xi_n^A, \xi_n^B < \xi_{n+1}^A, \xi_{n+1}^B$. Whether this approach can be generalized to objects that are finite in

all three dimensions remains to be seen. It is clear that general iterative schemes of the form $\{\xi\}_{i+1} = A^{-1}(\{\xi\}_i + R[\{\xi\}_i])$, where $R[\{\xi\}]$ is a nonlinear term, can be derived. The question is whether the condition number of A can be made sufficiently small for convergence and whether the computation time can be made reasonable.

In summary, we have reproduced the Helmholtz force density from microscopic but purely classical principles. This result establishes a connection between macroscopic and microscopic theories of electrostriction and other electrically induced forces in continuous media. It can be concluded that the forces $\mathbf{f}_a(\mathbf{r})$ and $\mathbf{f}_b(\mathbf{r})$, which appear in the standard Lorentz and Einstein-Laub force densities [6] but do not predict the correct strain should be understood only in the integral sense. This is similar to the vector of electric polarization $\mathbf{P}(\mathbf{r})$, which always gives correctly the total dipole moment of a finite body but should not be interpreted literally as a density of dipole moment. Just as the spatial integral of $\mathbf{P}(\mathbf{r})$ retains its validity for arbitrarily time-varying fields and beyond the linear approximation, the integrals of $\mathbf{f}_a(\mathbf{r})$ and $\mathbf{f}_b(\mathbf{r})$ are generally valid—but the functions themselves should not be interpreted pointwise. In contrast, the Helmholtz force density $\mathbf{f}_H(\mathbf{r})$ can be interpreted as a pointwise density of force (at least, in liquids or crystals with simple symmetry such as NaCl) but is unlikely to retain validity beyond statics and linear approximation.

APPENDIX: GENERAL EXPRESSION FOR THE ELECTROSTRICTION AND HELMHOLTZ FORCE DENSITY

In this Appendix, we provide expressions for the Helmholtz and the electrostriction force densities, which are applicable beyond the main assumptions adopted in this paper. In particular, these expressions can be used in the case of more general strain and stress tensors and, at least formally, in the case of nonlinear relation between \mathbf{P} and \mathbf{E} . However, the formulas should not be applied to strongly nonlinear phenomena such as spontaneous polarization in ferroelectrics, phase transitions and hysteresis. We also stay within the framework of linear elasticity (the relation between strain and stress is linear) as otherwise the theory becomes exceedingly complicated.

We have seen in Sec. II that the electrostatic force density can be decomposed into a term with nonvanishing volume integral, which yields the total force \mathbf{F}_{tot} according to (2), and a divergence of some tensor of rank 2, $\hat{T}(\mathbf{r})$, which vanishes outside of the body. The latter term integrates to zero. Under very general conditions, the force densities $\mathbf{f}_a(\mathbf{r})$, $\mathbf{f}_b(\mathbf{r})$ defined in (1) integrate to the same (correct) value \mathbf{F}_{tot} . All other force densities can be written as either $\mathbf{f}_a(\mathbf{r})$ or $\mathbf{f}_b(\mathbf{r})$ plus divergence of a tensor. If we start from $\mathbf{f}_a(\mathbf{r})$, the Helmholtz force density is of the form

$$\mathbf{f}_H(\mathbf{r}) = -(\nabla \cdot \mathbf{P}(\mathbf{r}))\mathbf{E}(\mathbf{r}) + \nabla \cdot \hat{T}(\mathbf{r}), \quad (\text{A1a})$$

where

$$\hat{T}(\mathbf{r}) = \mathbf{P}(\mathbf{r}) \otimes \mathbf{E}(\mathbf{r}) - \frac{1}{2}(\mathbf{P}(\mathbf{r}) \cdot \mathbf{E}(\mathbf{r}))\hat{I} + \frac{\hat{s}(\mathbf{r})}{8\pi}, \quad (\text{A1b})$$

and $\hat{s}(\mathbf{r})$ is the stress tensor associated with the effect of electrostriction. The factor of $1/8\pi$ has been introduced in (A1b) for later convenience and consistency with other notations. Expression (A1) does not yet contain the dielectric permittivity ϵ explicitly and can, at least formally, be applied to an arbitrary relation between $\mathbf{P}(\mathbf{r})$ and $\mathbf{E}(\mathbf{r})$.

In linear elasticity, the electrostrictive stress tensor $\hat{s}(\mathbf{r})$ is coupled to the electrostrictive strain $\hat{\sigma}(\mathbf{r})$ by the constitutive relations

$$\begin{aligned} s_{ij}(\mathbf{r}) &= C_{ijkl} \sigma_{kl}(\mathbf{r}), \\ \sigma_{ij}(\mathbf{r}) &= D_{ijkl} s_{kl}(\mathbf{r}), \end{aligned} \quad (\text{A2})$$

where summation over repeated indexes is implied. Here \hat{C} and \hat{D} are the stiffness (the elastic moduli) and the compliance tensors of the medium. The electrostrictive stress and strain are both quadratic in the electric field, viz,

$$\begin{aligned} s_{ij}(\mathbf{r}) &= \alpha_{ijkl} E_k(\mathbf{r})E_l(\mathbf{r}), \\ \sigma_{ij}(\mathbf{r}) &= \mu_{ijkl} E_k(\mathbf{r})E_l(\mathbf{r}). \end{aligned} \quad (\text{A3})$$

Here $\hat{\alpha}$ and $\hat{\mu}$ are the electrostrictive coefficients (tensors of rank 4). The relation between $\hat{\alpha}$ and $\hat{\mu}$ follows from the constitutive relations (A2):

$$\alpha_{ijkl} = C_{ijmn} \mu_{mnkl}, \quad \mu_{ijkl} = D_{ijmn} \alpha_{mnkl}. \quad (\text{A4})$$

The tensors $\hat{\alpha}$ and $\hat{\mu}$ in terms of derivatives of electric polarization of the medium with respect to the stress or strain and electric field can be obtained from various thermodynamic identities [14]. Specifically

$$\alpha_{ijkl} = -\frac{4\pi}{\partial \sigma_{ij} \partial E_l(\mathbf{r})} \frac{\partial^2 P_k(\mathbf{r})}{\partial \sigma_{ij} \partial E_l(\mathbf{r})}, \quad \mu_{ijkl} = -\frac{4\pi}{\partial s_{ij} \partial E_l(\mathbf{r})} \frac{\partial^2 P_k(\mathbf{r})}{\partial s_{ij} \partial E_l(\mathbf{r})}. \quad (\text{A5})$$

Here the derivative with respect to $E_l(\mathbf{r})$ is evaluated in every point in space. If the relation between $P_k(\mathbf{r})$ and $E_l(\mathbf{r})$ is nonlinear, the resulting electrostrictive coefficients are also \mathbf{r} -dependent and not truly linear coefficients of the medium. This is a serious complication. If however the polarization response is linear or we can linearize this relation for the relevant magnitudes of the electric field, we can write

$$\frac{\partial P_k(\mathbf{r})}{\partial E_l(\mathbf{r})} = \frac{\epsilon_{kl} - \delta_{kl}}{4\pi}. \quad (\text{A6})$$

In this case, the tensors $\hat{\alpha}$ and $\hat{\mu}$ are constant inside the medium and vanish in vacuum, as expected. From (A5) and (A6), we find

$$\alpha_{ijkl} = -\frac{\partial \epsilon_{kl}}{\partial \sigma_{ij}}, \quad \mu_{ijkl} = -\frac{\partial \epsilon_{kl}}{\partial s_{ij}}. \quad (\text{A7})$$

These relations are applicable to linear but arbitrarily anisotropic media.

We now return to the model of this paper in which only uniform uniaxial strain along the Z axis is present. The only relevant elements of $\hat{\sigma}$ and \hat{s} are in this case σ_{zzzz} and s_{zzzz} , which we denote by σ and s for simplicity. For a uniform strain along Z , σ and s are of the form $\sigma = \Lambda/\Lambda_0 - 1$ and $s = -\Pi_{\text{ext}} = -(k/h)p$, where Π_{ext} is the external pressure (positive if it tries to compress the slab and negative otherwise). We then find

$$\alpha = \frac{\partial \epsilon}{\partial \sigma} = -\Lambda_0 \frac{\partial \epsilon}{\partial \Lambda}, \quad \mu = -\frac{\partial \epsilon}{\partial s} = \frac{h}{k} \frac{\partial \epsilon}{\partial p}. \quad (\text{A8})$$

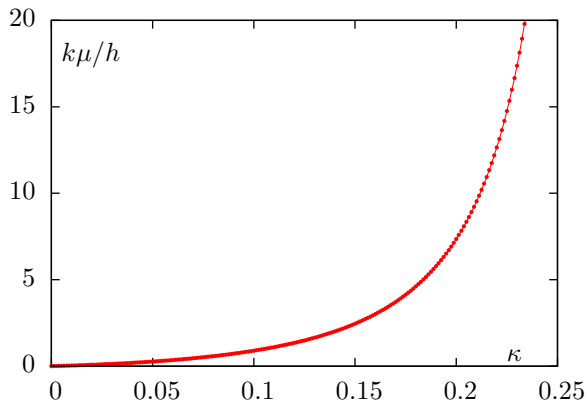


FIG. 13. Electrostrictive coefficient μ as a function of κ . $N = 150$.

In view of the constitutive relation $s = \eta\sigma$, only two of these three parameters are independent and in principle it is sufficient to compute numerically only two of them. Above, we computed the parameters η and α as functions of the model parameter κ (Figs. 8 and 11). For consistency, we can also compute μ using the second equation in (A8). This computation does not utilize the constitutive relation directly and is therefore independent. We display the electrostrictive coefficient μ as a function of κ computed using the second equation in (A8) in Fig. 13. The derivative was computed using two points $p = 0$ and $p = \delta p = 0.001$. Note that the data of Figs. 8 (Young's modulus η), Fig. 11 (electrostrictive coefficient α) and Fig. 13 (electrostrictive coefficient μ) satisfy the constitutive relation with the relative precision 10^{-6} . That is, the computed values satisfy $|\mu\eta/\alpha - 1| < 10^{-6}$ for all κ 's used. This provides an additional consistency check for the simulations.

-
- [1] B. Anghinoni, G. Flizikowski, L. Malacarne, M. Partanen, S. E. Bialkowski, and N. G. C. Astrath, *Ann. Phys.* **443**, 169004 (2022).
- [2] M. Mansuripur, *Opt. Commun.* **284**, 594 (2011).
- [3] K. J. Chau and H. J. Lezec, *Appl. Phys. A* **105**, 267 (2011).
- [4] I. Brevik, *Int. J. Mod. Phys. A* **34**, 1941003 (2019).
- [5] V. A. Markel, *Ann. Phys.* **422**, 168293 (2020).
- [6] M. Mansuripur, *Appl. Phys. A* **123**, 653 (2017).
- [7] H. Helmholtz, *Ann. Phys.* **249**, 385 (1881).
- [8] S. M. Barnett and R. Loudon, *J. Phys. B* **39**, S671 (2006).
- [9] P. W. Tasker, *J. Phys. C: Solid State Phys.* **12**, 4977 (1979).
- [10] M. Springborg and B. Kirtman, *Can. J. Chem.* **87**, 984 (2009).
- [11] See Supplemental Material at <http://link.aps.org/supplemental/10.1103/PhysRevB.107.104307> for a computational package and scripts that can be used to re-compute all data of this paper.
- [12] Beyond quasi-statics, we must also account for radiative reaction. In this case, the densities $\mathbf{f}_a(\mathbf{r})$ and $\mathbf{f}_b(\mathbf{r})$ are not sufficient to predict the total force even in non-magnetic media.
- [13] The condition of stationarity is used in the theory and simulations of this paper. However, some statements hold more generally. For example, the relation (3) does not require stationarity. In contrast, the relation (7) is valid only for static fields.
- [14] F. Li, L. Jin, Z. Xu, and S. Zhang, *Appl. Phys. Rev.* **1**, 011103 (2014).
- [15] W. K. H. Panofsky and M. Phillips, *Classical Electricity and Magnetism* (Addison-Wesley Pub., Reading, MA, 1962).
- [16] I. E. Tamm, *Fundamentals of the Theory of Electricity* (Mir, Moscow, 1979).
- [17] L. D. Landau and L. P. Lifshitz, *Electrodynamics of Continuous Media* (Pergamon Press, Oxford, UK, 1984).
- [18] B. S. Park, H. S. Choi, J. O. Park, J. H. Wang, and I. H. Park, *IEEE Trans. Magnetics* **56**, 7515004 (2020).
- [19] M. Springborg, M. Zhou, M. Molayem, and B. Kirtman, *J. Phys. Chem. C* **122**, 11926 (2018).
- [20] M. Springborg, V. Tevekeliyska, and B. Kirtman, *Phys. Rev. B* **82**, 165442 (2010).
- [21] M. Springborg and B. Kirtman, *Theor. Chem. Acc.* **130**, 687 (2011).
- [22] P. P. Ewald, *Ann. Phys.* **369**, 253 (1921).
- [23] D. E. Parry, *Surf. Sci.* **49**, 433 (1975).
- [24] I. Tsukerman, *IEEE Trans. Magn.* **40**, 2158 (2004).
- [25] S. Rostami, S. A. Ghasemi, and E. N. Oskoe, *J. Chem. Phys.* **145**, 124118 (2016).
- [26] V. A. Markel, *J. Opt. Soc. Am. A* **33**, 2237 (2016).
- [27] I. Tsukerman, *Rev. Phys.* **7**, 100061 (2021).
- [28] K. Uchino, S. Nomura, K. Vedam, R. E. Newnham, and L. E. Cross, *Phys. Rev. B* **29**, 6921 (1984).
- [29] M. Partanen, B. Anghinoni, N. G. C. Astrath, and J. Tulkki, *Phys. Rev. A* **107**, 023525 (2023).